Reconstruction of secular variation in seawater sulfate concentrations

T.J. Algeo[1,2,3]*, G.M. Luo[2], H.Y. Song[3], T.W. Lyons[4], and D.E. Canfield[5]

[1]Department of Geology, University of Cincinnati, Cincinnati, Ohio 45221-0013, U.S.A.
[2] State Key Laboratory of Geological Processes and Mineral Resources, China University of Geosciences, Wuhan, 430074, China
[3]State Key Laboratory of Biogeology and Environmental Geology, China University of Geosciences, Wuhan, 430074, China
[4]Department of Earth Sciences, University of California, Riverside, California 92521-0423, U.S.A.
[5]Nordic Center for Earth Evolution (NordCEE) and Institute of Biology, University of Southern Denmark, Campusvej 55, 5230 Odense M, Denmark

*Correspondence to: T. J. Algeo (Email: Thomas.Algeo@uc.edu)

Abstract

Long-term secular variation in seawater sulfate concentrations ($[SO_4^{2-}]_{SW}$) is of interest owing to its relationship to the oxygenation history of Earth's surface environment. In this study, we develop two complementary approaches for quantification of sulfate concentrations in ancient seawater and test their application to late Neoproterozoic (635 Ma) to Recent marine units. The "rate method" is based on two measurable parameters of paleomarine systems: (1) the S-isotope fractionation associated with microbial sulfate reduction (MSR), as proxied by $\Delta^{34}S_{CAS-PY}$, and (2) the maximum rate of change in seawater sulfate, as proxied by $\partial\delta^{34}S_{CAS}/\partial t(max)$. The "MSR-trend method" is based on the empirical relationship of $\Delta^{34}S_{CAS-PY}$ to aqueous sulfate concentrations in 81 modern depositional systems. For a given paleomarine system, the rate method yields an estimate of maximum possible $[SO_4^{2-}]_{SW}$ (although results are dependent on assumptions regarding the pyrite burial flux, F_{PY}), and the MSR-trend method yields an estimate of mean $[SO_4^{2-}]_{SW}$. An analysis of seawater sulfate concentrations since 635 Ma suggests that $[SO_4^{2-}]_{SW}$ was low during the late Neoproterozoic (<5 mM), rose sharply across the Ediacaran/Cambrian boundary (~5-10 mM), and rose again during the Permian (~10-30 mM) to levels that have varied only slightly since 250 Ma. However, Phanerozoic seawater sulfate concentrations may have been drawn down to much lower levels (~1-4 mM) during short (<~2-Myr) intervals of the Cambrian, Early Triassic, Early Jurassic, and Cretaceous as a consequence of widespread ocean anoxia, intense MSR, and pyrite burial. The procedures developed in this study offer potential for future high-resolution quantitative analyses of paleoseawater sulfate concentrations.

Keywords: Phanerozoic; Neoproterozoic; microbial sulfate reduction; pyrite; carbonate-associated sulfate; sulfur cycle

1 Introduction

Oceanic sulfate plays a key role in the biogeochemical cycles of S, C, O and Fe (Canfield, 1998; Lyons and Gill, 2010; Halevy et al., 2012; Planavsky et al., 2012). For example, >50% of organic matter and methane in marine sediments is oxidized via processes linked to microbial sulfate reduction (MSR) (Jørgensen, 1982; Valentine, 2002). At a concentration of ~29 mM in the modern ocean, sulfate is the second most abundant anion in seawater (Millero, 2005). Its concentration is an important proxy for seawater chemistry and the oxidation state of the Earth's atmosphere and oceans (Kah et al., 2004; Johnston, 2011).

Although there is broad agreement that seawater sulfate concentrations have increased through time, the history of its accumulation remains poorly known in detail. Archean and Early Proterozoic oceans are thought to have had very limited sulfate inventories (<200 μM), as implied by small degrees of sulfate-sulfide and mass-independent S-isotope fractionation (Shen et al., 2001; Strauss, 2003; Farquhar et al., 2007; Adams et al., 2010; Johnston, 2011; Owens et al., 2013; Luo et al., 2015). The accumulation of atmospheric O_2 during the 'Great Oxidation Event' (~2.3-2.0 Ga; Holland, 2002; Bekker et al., 2004) is thought to have resulted in a long-term increase in seawater sulfate concentrations (Canfield and Raiswell, 1999; Canfield et al., 2007; Kah et al., 2004; Fike et al., 2006). However, this increase was probably not monotonic and declines in pO$_2$ may have resulted in one or more seawater sulfate minima between ~1.9 and 0.6 Ga (Planavsky et al., 2012; Luo et al., 2015). Estimates of Phanerozoic seawater sulfate concentrations are uniformly higher, although there is no consensus regarding exact values. Fluid inclusion data yielded estimates of ~10 to 30 mM for most of the Phanerozoic (Horita et al., 2002; Lowenstein et al., 2003, 2005). However, recent S-isotope studies have modeled concentrations as low as ~1-5 mM during portions of the Cambrian, Triassic, Jurassic, and Cretaceous (Wortmann and Chernyavsky, 2007; Adams et al., 2010; Luo et al., 2010; Gill et al., 2011a,b; Newton et al., 2011; Owens et al., 2013; Song et al., 2014), and a recent marine S-cycle model yielded low concentrations (<10 mM) for much of the Cretaceous and Early Cenozoic before a rise to near-modern levels at ~40 Ma (Wortmann and Paytan, 2012).

Here, we develop two approaches for quantitative analysis of seawater sulfate concentrations ([SO$_4^{2-}$]$_{SW}$) in paleomarine systems. The first method calculates a maximum possible [SO$_4^{2-}$]$_{SW}$ based on a combination of two parameters that are readily measurable in most paleomarine systems: (1) the S-isotope fractionation between cogenetic sedimentary sulfate and sulfide (Δ^{34}S$_{CAS-PY}$), and (2) the maximum observed rate of variation in seawater sulfate δ^{34}S ($\partial\delta^{34}$S$_{CAS}/\partial t$). This rate-based method is an extension of earlier modeling work by Kump and Arthur (1999), Kurtz et al. (2003), Kah et al. (2004), Bottrell and Newton (2006), and Gill et al. (2011a,b). The second approach yields an estimate of mean seawater [SO$_4^{2-}$] based on an empirical relationship between Δ^{34}S$_{CAS-PY}$ and aqueous sulfate concentrations (the "MSR trend") in 81 modern depositional systems. Conceptually, the MSR-trend method is related to the fractionation relationship given in Habicht et al. (2002; their figure 1). Although some earlier studies have made qualitative assessments of paleo-seawater [SO$_4^{2-}$], the significance of our methodology is that the [SO$_4^{-2}$] of ancient seawater can be quantitatively constrained as a function of measurable sediment parameters and empirical fractionation relationships.

84   We fully recognize that the marine sulfur cycle is controlled by myriad factors, many of
85   which are only now coming to light thanks to detailed field and laboratory studies, and that not
86   all such influences can be thoroughly considered and accommodated in the present study.
87   While acknowledging the complexity of the sulfur cycle, this study attempts to identify broad
88   first-order trends that potentially transcend these diverse influences and that are robust over
89   significant intervals of geologic time. Our ultimate goal is to generate useful approximations of
90   the long-term history of sulfate in the ocean. Our results suggest that large-scale empirical
91   relationships may exist that are not highly sensitive to influences such as organic substrate
92   type, sulfate reduction rates, strain-specific fractionation, and other factors. We envision such
93   local influences, as they become more completely understood, being mapped onto, and thus
94   integrated with, the broad first-order relationships documented in this study.

95

2 Methods of modeling paleo-seawater sulfate concentrations

2.1 The rate method

98   The marine S cycle has a limited number of fluxes with fairly well-defined S-isotope ranges
99   (Holser et al., 1989; Canfield, 2004; Bottrell and Newton, 2006), making it amenable to analysis
100   through modeling (e.g., Halevy et al., 2012). Subaerial weathering yields a riverine sulfate
101   source flux (F_Q) of ~10 x 10^{13} g yr^{-1} with an average $\delta^{34}S$ of ~+6‰, which is significantly lighter
102   than the modern seawater sulfate $\delta^{34}S$ of +20‰. Sulfate is removed to the sediment either in
103   an oxidized state, as carbonate-associated sulfate (CAS) or evaporite deposits, or in a reduced
104   state, mainly as FeS or FeS_2. The oxidized sink has a flux (F_{EVAP}) of ~6 x 10^{13} g yr^{-1} with a S-
105   isotopic composition that closely mimics that of coeval seawater ($\Delta^{34}S_{SW-EVAP}$ of -4 to 0‰). The
106   reduced sink has a flux (F_{PY}) of ~4 x 10^{13} g yr^{-1} with a composition that characteristically shows a
107   large negative fractionation relative to coeval seawater ($\Delta^{34}S_{sulfate-sulfide}$ of ~30 to 60‰; Habicht
108   and Canfield, 1997; Canfield, 2001; Brüchert, 2004; Brunner and Bernasconi, 2005). Secular
109   variation in seawater sulfate $\delta^{34}S$ is mainly due to changes in the relative size of the sink fluxes,
110   with increasing (decreasing) burial of pyrite relative to sulfate leading to more (less) ^{34}S-
111   enriched seawater sulfate (Holser et al., 1989; Bottrell and Newton, 2006; Halevy et al., 2012).

112   The rate method calculates a maximum seawater sulfate concentration ($[SO_4^{2-}]_{SW}(max)$)
113   based on two parameters: (1) S-isotope fractionation between cogenetic sedimentary sulfate
114   and sulfide ($\Delta^{34}S_{sulfate-sulfide}$, as proxied by $\Delta^{34}S_{CAS-PY}$), and (2) the maximum observed rate of
115   variation in seawater sulfate S isotopes ($\partial\delta^{34}S_{SO4}/\partial t(max)$, as proxied by $\partial\delta^{34}S_{CAS}/\partial t(max)$) (Fig.
116   1). Rates of isotopic change for seawater sulfate are given by:

117   $$\partial\delta^{34}S_{CAS}/\partial t \ = \ ((F_Q \times \Delta^{34}S_{Q-SW}) - (F_{PY} \times \Delta^{34}S_{CAS-PY})) \ / \ M_{SW} \qquad (1)$$

118   where $F_Q \times \Delta^{34}S_{Q-SW}$ is the flux-weighted difference in the isotopic compositions of the source
119   flux and seawater (SW), $F_{PY} \times \Delta^{34}S_{CAS-PY}$ is the flux-weighted difference in the isotopic
120   compositions of the reduced-S sink flux and seawater, and M_{SW} is the mass of seawater sulfate.
121   The full expression represents the time-integrated influence of the source and sink fluxes on
122   seawater sulfate $\delta^{34}S$. The maximum possible rate of change in the sulfur isotopic composition
123   of seawater sulfate is attained when the source flux goes to zero:

124 $$\partial\delta^{34}S_{CAS}/\partial t(max) = F_{PY} \times \Delta^{34}S_{CAS-PY} / M_{SW} \tag{2}$$

125 Reorganization of this equation allows calculation of a maximum seawater sulfate
126 concentration from measured values of $\Delta^{34}S_{CAS-PY}$ and $\partial\delta^{34}S_{CAS}/\partial t(max)$:

127 $$M_{SW} = k_1 \times F_{PY} \times \Delta^{34}S_{CAS-PY} / \partial\delta^{34}S_{CAS}/\partial t(max) \tag{3}$$

128 $$[SO_4{}^{2-}]_{SW}(max) = k_2 \times M_{SW} \tag{4}$$

129 where k_1 is a unit-conversion constant equal to 10^6, and k_2 is a constant relating the mass of
130 seawater sulfate to its molar concentration that is equal to 2.22×10^{-20} mM g^{-1}. Kah et al.
131 (2004) assumed $F_{PY} = 10 \times 10^{13}$ g yr^{-1}, which is the total sink flux for modern seawater sulfate, in
132 order to model $\partial\delta^{34}S_{CAS}/\partial t(max)$. While this may be appropriate for intervals of widespread
133 euxinia in the global ocean, $F_{PY} = 4 \times 10^{13}$ g yr^{-1} (i.e., the modern sink flux) may better represent
134 intervals with well-oxygenated oceans in which the sink fluxes of sulfate S and pyrite S are both
135 substantial (Fig. 1). Assuming $F_{PY} = 4 \times 10^{13}$ g yr^{-1} and values of $\Delta^{34}S_{CAS-PY}$ and $\partial\delta^{34}S_{CAS}/\partial t(max)$
136 potentially representative of modern marine systems (e.g., 35‰ and 1.1‰ Myr^{-1}, respectively),
137 Equation 3 yields the modern seawater sulfate mass of $M_{SW} = 1.3 \times 10^{21}$ g and Equation 4 yields
138 the modern seawater sulfate concentration of ~29 mM.

139   Relationships among the rate-method parameters are illustrated in Figure 1 for $\Delta^{34}S_{CAS-}$
140 $_{PY}$ from 1 to 100‰ (ordinal scale) and for discrete values of $\partial\delta^{34}S_{CAS}/\partial t(max)$ ranging from 1 to
141 100‰ Myr^{-1} (diagonal lines). $[SO_4{}^{-2}]_{SW}$ increases linearly with increasing $\Delta^{34}S_{CAS-PY}$ (at constant
142 $\partial\delta^{34}S_{CAS}/\partial t(max)$) and decreases linearly with increasing $\partial\delta^{34}S_{CAS}/\partial t(max)$ (at constant $\Delta^{34}S_{CAS-}$
143 $_{PY}$). The *measured* maximum $\partial\delta^{34}S_{CAS}/\partial t$ for a paleomarine unit is generally smaller than the
144 *theoretical* maximum $\partial\delta^{34}S_{SO4}/\partial t$ because the latter can be achieved only when the source flux
145 of seawater sulfur is reduced (at least transiently) to zero (Kah et al., 2004), which does not
146 routinely occur in nature. As a consequence, rate-method estimates of $[SO_4{}^{2-}]_{SW}$ are generally
147 larger than actual seawater sulfate concentrations, so Equation 4 yields the *maximum* likely
148 $[SO_4{}^{2-}]_{SW}$ for a paleomarine unit of interest. This outcome can be illustrated by a calculation for
149 the modern ocean, using $\Delta^{34}S_{CAS-PY}$ of ~30-60‰ and $\partial\delta^{34}S_{CAS}/\partial t(max)$ of ~0.7‰ Myr^{-1} (based on
150 the Cenozoic seawater sulfate $\delta^{34}S$ record; Paytan et al., 1998). These inputs yield
151 $[SO_4{}^{2-}]_{SW}(max)$ values between ~40 and 80 mM, which is modestly larger than the actual
152 modern $[SO_4{}^{2-}]_{SW}$ of ~29 mM (Fig. 1). Overestimation of modern $[SO_4{}^{2-}]_{SW}$ is due to measured
153 $\partial\delta^{34}S_{CAS}/\partial t$ values for the Cenozoic (≤ 0.7‰ Myr^{-1}) being lower than the theoretical maximum
154 for modern seawater (~1-2‰ Myr^{-1}; Fig. 1). This situation is probably typical of marine units of
155 all ages—measured rates of $\delta^{34}S_{CAS}$ variation will be lower than the theoretical maximum
156 because the source flux of sulfur to the oceans rarely if ever goes to zero.

157   The results of the rate method depend on the parameterization of the pyrite burial flux
158 (F_{PY}). This method is likely to yield an accurate estimate of seawater sulfate concentrations
159 only if F_{PY} is inversely proportional to the residence time of sulfate in seawater (τ_{SO4}), which
160 basically requires the marine sulfate system to be in equilibrium. If a value for F_{PY} is chosen
161 that is much larger or smaller than the equilibrium flux, then seawater sulfate concentrations
162 will be overestimated or underestimated, respectively (see Appendix B1 for extended
163 discussion). Second, the pyrite burial flux has almost certainly varied through time. Since pyrite
164 burial flux is a component of Equations 2 and 3, variations in this parameter will influence

165 calculated seawater sulfate concentrations. Phanerozoic variation in pyrite burial fluxes has
166 been calculated in several global carbon-sulfur cycle models (e.g., Berner, 2004; Bergmann et
167 al., 2004), although the details remain unpublished. We therefore explored the effects of
168 variable pyrite burial fluxes on seawater sulfate estimates by using the $[SO_4^{2-}]_{SW}$-dependent
169 pyrite burial flux relationship of Wortmann and Chernyavsky (2007). This procedure yielded
170 Phanerozoic $[SO_4^{2-}]_{SW}$ estimates that are close (±10%) to our original values (see Appendix B2
171 for extended discussion).

172

2.2 The MSR-trend method

174 An alternative approach to constraining ancient seawater sulfate concentrations is based on an
175 empirical relationship to S-isotope fractionation associated with microbial sulfate reduction
176 (F_{MSR}). We evaluated this relationship by compiling $\Delta^{34}S_{sulfate-sulfide}$ and $[SO_4^{2-}]_{aq}$ data for 81
177 modern depositional systems (Table A1; cf. Habicht et al., 2002). Each system was classified (1)
178 by salinity, as freshwater (<10 psu), brackish (10-30 psu), marine (30-40 psu), or hypersaline
179 (>40 psu; n.b., psu = practical salinity units), and (2) by redox conditions, as oxic or euxinic
180 depending on whether the chemocline was within the sediment or the watermass, respectively.

181   In the interests of applying uniform criteria to the generation of this dataset, we
182 followed a specific protocol. First, we adopted a modern seawater sulfate concentration of
183 2775 mg L^{-1}, or 28.9 mM at an average seawater density of 1025 kg m^{-3} (Millero, 2005). For
184 brackish marine watermasses, we used measured aqueous sulfate concentrations or, if
185 unavailable, estimated dissolved sulfate concentrations from salinity data:

186      $$[SO_4^{2-}] \ = \ [SO_4^{2-}]_{SW} \times S \, / \, S_{SW}$$
187   (5)

188 where $[SO_4^{2-}]$ and S are the sulfate concentration and salinity of the watermass of interest,
189 respectively, and S_{SW} is the salinity of average seawater (35 psu). Second, we used only in-situ
190 water-column measurements of aqueous sulfate $\delta^{34}S$. Third, we used sulfide $\delta^{34}S$ values either
191 from aqueous H_2S or from sedimentary sulfide proxies located within a few centimeters of the
192 sediment-water interface, thus avoiding sedimentary sulfides that might be significantly ^{34}S-
193 enriched owing to sulfate-limited burial conditions (Kaplan et al., 1963; Canfield et al., 1992).
194 However, some variation in $\delta^{34}S$ among cogenetic early-formed sedimentary sulfides is
195 common. Acid-volatile sulfur (AVS, consisting mainly of monosulfides; Rickard, 1975) tends to
196 have a lighter sulfur isotopic composition, closer to that of the instantaneously generated H_2S
197 at a given sediment depth, because it converts quickly to pyrite (Zaback and Pratt, 1992; Lyons,
198 1997). On the other hand, organic sulfur tends to be isotopically heavier owing to late-stage
199 sulfurization of organic matter or, possibly, to fractionations associated with sulfur uptake
200 (Zaback and Pratt, 1992; Werne et al., 2000, 2003, 2008). Although our dataset includes a
201 combination of pyrite, AVS, total reduced sulfur (TRS), and aqueous H_2S sulfur isotopic data
202 owing to variations in sample analysis among published studies, it is weighted toward pyrite
203 data (n = 48 out of a total of 81; Table A1). An analysis of $\Delta^{34}S_{sulfate-sulfide}$ variation among the
204 multiple sulfide sources used in our study revealed no statistically significant differences (see
205 Appendix B3). Because pyrite $\delta^{34}S$ is frequently analyzed in paleomarine studies, our MSR trend

206 (Fig. 2) should be widely applicable to an analysis of paleoseawater sulfate concentrations. One
207 caveat in this regard is that $\Delta^{34}S_{CAS-PY}$ estimates for paleomarine units should be based on
208 syngenetic or early diagenetic pyrite, as determined by well-established petrographic and
209 geochemical criteria (e.g., Wilkin et al., 1996; Lyons and Severmann, 2006).

210 The protocol described above produced an internally consistent dataset (Table A1) that
211 exhibits a pronounced relationship between $\Delta^{34}S_{sulfate-sulfide}$ and $[SO_4^{2-}]_{aq}$ (Fig. 2a). Regression of
212 $\Delta^{34}S_{sulfate-sulfide}$ on $[SO_4^{2-}]_{aq}$ yields a strong positive relationship ($r = +0.90$, $p(\alpha) <0.01$). The
213 trend represents an increase in $\Delta^{34}S_{sulfate-sulfide}$ from ~4-6‰ at 0.1 mM to ~30-60‰ at 29 mM
214 (i.e., modern seawater $[SO_4^{2-}]$). $\Delta^{34}S_{sulfate-sulfide}$ appears to peak at $[SO_4^{2-}]_{aq}$ of 15-20 mM, with a
215 mean value ~5-10‰ greater than for $[SO_4^{2-}]_{aq}$ of 29 mM , but this effect is small relative to the
216 overall relationship between $\Delta^{34}S_{sulfate-sulfide}$ and $[SO_4^{2-}]_{aq}$, and we did not factor it separately
217 into the regression analysis. For hypersaline environments in which $[SO_4^{2-}]_{aq} >29$ mM,
218 $\Delta^{34}S_{sulfate-sulfide}$ does not continue to rise but, rather, shows roughly the same range as for
219 modern seawater (Fig. 2a). Finally, we analyzed the data by redox environment and found only
220 minor and statistically insignificant differences between oxic and euxinic settings (n.b.,
221 hypersaline environments were not included in this analysis). The distributions of the oxic and
222 euxinic datasets show broad overlap (Fig. 2a), so benthic redox conditions appear to exhibit no
223 discernible influence on the relationship of $\Delta^{34}S_{sulfate-sulfide}$ to $[SO_4^{2-}]_{aq}$.

224 Our analysis demonstrates that a strong relationship exists between F_{MSR} and $[SO_4^{2-}]_{aq}$
225 in natural aqueous systems ($r = +0.90$, $p(\alpha) <0.01$; Fig. 2a). Our results are similar to, although
226 more linear and more statistically robust than, those reported by Habicht et al. (2002) on the
227 basis of culture experiments. We recognize that there are multiple environmental and
228 physiological controls on fractionation by sulfate reducers (see Section 3), and that under
229 certain natural and experimental conditions the relationship of F_{MSR} to $[SO_4^{2-}]_{aq}$ can deviate
230 markedly from that in our dataset. However, the pattern of covariation between F_{MSR} and
231 $[SO_4^{2-}]_{aq}$ documented here represents a robust relationship that appears to hold for a wide
232 range of natural environments, reflecting the possibly near-ubiquitous influence of $[SO_4^{2-}]_{aq}$ on
233 F_{MSR}. The apparent breakdown of this relationship in hypersaline environments (Fig. 2a) needs
234 further testing; our dataset for hypersaline environments is too small (n = 6) to reach firm
235 conclusions. However, the strength of the F_{MSR}-$[SO_4^{2-}]_{aq}$ relationship for watermasses with
236 salinities ranging up to ~40 psu suggests that it can serve as a basis for evaluating the $[SO_4^{2-}]_{aq}$
237 of ancient seawater. Seawater $[SO_4^{2-}]$ can be estimated graphically by projecting measured
238 values of $\Delta^{34}S_{CAS-PY}$ from the ordinal scale to the MSR trend and then to the abscissa (Fig. 2b), or
239 by using the following empirical equation:

240 $$\log[SO_4^{2-}] = (\log(\Delta^{34}S_{CAS-PY}) - 1.10) / 0.42 \qquad (6)$$

241 The upper and lower uncertainty limits for estimates of seawater $[SO_4^{2-}]$ based on this
242 relationship are:

243 $$\log[SO_4^{2-}] = (\log(\Delta^{34}S_{CAS-PY}) - 1.18) / 0.40 \quad \text{(upper limit)} \qquad (7)$$

244 $$\log[SO_4^{2-}] = (\log(\Delta^{34}S_{CAS-PY}) - 1.02) / 0.44 \quad \text{(lower limit)} \qquad (8)$$

245 In order to account for uncertainties in $\Delta^{34}S_{CAS-PY}$ as well as the F_{MSR} regression, estimates of
246 minimum $[SO_4^{2-}]_{SW}$ should make use of minimum $\Delta^{34}S_{CAS-PY}$ values in combination with the
247 upper uncertainty limit equation (Eq. 7), and estimates of maximum $[SO_4^{2-}]_{SW}$ should make use
248 of maximum $\Delta^{34}S_{CAS-PY}$ values in combination with the lower uncertainty limit equation (Eq. 8;
249 Fig. 2b).
250

3 Controls on fractionation by microbial sulfate reducers

252 The biogeochemical nature of the microbial sulfate reduction (MSR) process and its associated
253 S-isotope fractionations have been extensively investigated in earlier studies. Sulfate reducers
254 preferentially utilize sulfate containing ^{32}S during dissimilatory reduction to hydrogen sulfide in
255 conjunction with the anaerobic decay of organic matter (Kaplan, 1983; Canfield, 2001; Bradley
256 et al., 2011). The exact controls on this isotopic discrimination continue to be a topic of intense
257 debate. The paradigmatic view is that this fractionation is mainly a kinetic effect associated
258 with the rate-limiting step for intracellular sulfate processing, although it is known that
259 fractionation also may accompany sulfate transport across the cell membrane (Rees, 1973;
260 Detmers et al., 2001; Brüchert, 2004; Bradley et al., 2011). The kinetic effect is thought to be
261 dependent on aqueous sulfate concentrations, with substantially larger fractionations
262 associated with $[SO_4^{2-}]_{aq}$ >~200 µM (Habicht et al., 2002; Gomes and Hurtgen, 2013; but see
263 Canfield, 2001, for a counter example). Rees (1973) proposed a maximum discrimination of
264 46‰ but the theoretical basis for this value was re-assessed by Brunner and Bernasconi (2005).
265 Recent studies have documented F_{MSR} as large as 66‰ in culture experiments (Sim et al.,
266 2011a) and 70-80‰ in natural systems (Rudnicki et al., 2001; Wortmann et al., 2001; Canfield
267 et al., 2010). Even larger fractionations have been reported but are generally considered to be
268 the result of multistage disproportionation of intermediate-oxidation-state sulfur compounds
269 (Canfield and Thamdrup, 1994).

270   Investigations of natural and experimental systems have documented a number of
271 additional controls on F_{MSR}. One of the most important controls is f_{SO4}, i.e., the fraction of
272 remaining dissolved sulfate (Gomes and Hurtgen, 2013). In 'open systems' containing a high
273 concentration of dissolved sulfate (e.g., the modern ocean), f_{SO4} does not vary measurably from
274 1.0 because the quantity of sulfate converted to sulfide via MSR is a small fraction of the total
275 aqueous sulfate inventory. In this case, the produced sulfide will show the maximum degree of
276 fractionation, which is typically ~30 to 60‰ in modern marine systems (Fig. 2a; Table A1). In
277 contrast, in 'closed systems' in which the aqueous sulfate inventory is limited (e.g., sediment
278 porewaters or low-sulfate freshwater systems), dissolved sulfate concentrations can be
279 substantially reduced or completely depleted through MSR, causing f_{SO4} to evolve toward zero.
280 As $[SO_4^{2-}]_{aq}$ becomes smaller, sulfate reducers utilize a progressively larger fraction of the total
281 dissolved sulfate pool, reducing the effective fractionation to small values (Habicht et al., 2002;
282 Gomes and Hurtgen, 2013). In these settings, the aggregate $\delta^{34}S$ composition of the produced
283 sulfide approaches that of the original aqueous sulfate inventory, and $\Delta^{34}S_{sulfate-sulfide}$
284 approaches zero (Kaplan, 1983; Habicht et al., 2002). In a macro sense, f_{SO4} can be proxied by
285 $[SO_4^{2-}]_{aq}$, accounting for the strong first-order relationship between the latter parameter and

286    $\Delta^{34}S_{sulfate-sulfide}$ ($r = +0.90$, $p(\alpha)$ <0.01; Fig. 2a). However, not all researchers agree on the

287   importance of f_{SO4} as a control on F_{MSR} (e.g., Leavitt et al., 2013).

288   Other factors may influence F_{MSR} under certain conditions. First, different dissimilatory

289   reduction pathways yield different isotopic discriminations. Oxidation of organic substrates to

290   CO_2 yields larger fractionations (~30-60‰) than oxidation to acetate (<18‰) (Detmers et al.,

291   2001; Brüchert et al., 2001; Brüchert, 2004). Incomplete oxidation of organic substrates is a

292   feature characteristic of sulfate reducers in hypersaline environments (Habicht and Canfield,

293   1997; Oren, 1999; Detmers et al., 2001; Stam et al., 2010) and may account for the somewhat

294   smaller fractionations typically encountered in such environments (Fig. 2a). Second, the type of

295   organic substrate also matters, as ethanol, lactate, glucose, and other compounds yield

296   different fractionations under otherwise similar conditions (Canfield, 2001; Detmers et al.,

297   2001; Kleikemper et al., 2004; Sim et al., 2011b). Third, sulfate reduction rates may also

298   influence F_{MSR}, with higher rates associated with smaller isotopic discriminations (Kaplan and

299   Rittenberg, 1964; Kemp and Thode, 1968; Rees, 1973; Chambers et al., 1975; Habicht and

300   Canfield, 1996; Brüchert et al., 2001; Canfield, 2001; Brunner and Bernasconi, 2005). Recent

301   experiments by Leavitt et al. (2013) showed that F_{MSR} declines rapidly with increasing sulfate

302   reduction rates before leveling off at ~15-20‰ at rates >50 mmol H_2S per unit substrate per

303   day. Habicht and Canfield (2001) hypothesized that F_{MSR} is only incidentally related to sulfate

304   reduction rates because both are correlated with the disproportionation of intermediate-

305   oxidation-state S compounds by sulfur-oxidizing bacteria, which have probably been present

306   since the Archean (Johnston et al., 2005; Wacey et al., 2010). Fourth, cell external sulfide (CES)

307   concentrations, when high, can cause back-diffusion of sulfide into cells, with subsequent

308   oxidative recycling to sulfate (Brunner and Bernasconi, 2005; Eckert et al., 2011). Finally,

309   temperature has been shown to affect F_{MSR} in some studies (e.g., Canfield et al., 2006) but not

310   others (e.g., Detmers et al., 2001). The influence of temperature on F_{MSR} may operate through

311   the species-specific temperature dependence of enzymes.

312   Research to date clearly shows that controls on microbial sulfate reduction are complex

313   and incompletely understood. This situation reflects the diverse composition of the microbial

314   communities that process sulfur in the marine environment and the range of isotopic

315   fractionations associated with those processes (Brüchert, 2004). Yet even though multiple

316   environmental and physiological factors influence F_{MSR}, the strength of its relationship to

317    $[SO_4^{2-}]_{aq}$, as documented in this study (Fig. 2a), implies that aqueous sulfate concentrations are

318   the dominant first-order control on F_{MSR}, and that other factors such as organic substrate, rates

319   of MSR, and temperature are second-order controls whose effects may be randomized at a

320   larger scale and do not obscure the dominant influence of $[SO_4^{2-}]_{aq}$ in most environments.

321   Whether the quantitative form of our F_{MSR}-$[SO_4^{2-}]_{aq}$ relationship is unique to the present or

322   valid for the geologic past is unclear. Microbial S-cycling processes are thought to have been

323   conservative through time (e.g., Wacey et al., 2010), although lower atmospheric pO_2 prior to

324   ~635 Ma may have limited disproportionation of intermediate-oxidation-state sulfur

325   compounds and, thus, the potential for large fractionations (Habicht and Canfield, 2001;

326   Sørensen and Canfield, 2004; Johnston et al., 2005). In the following analysis, we adopt the

327   F_{MSR}-$[SO_4^{2-}]_{aq}$ relationship of Figure 2a as a basis for evaluating the $[SO_4^{2-}]_{aq}$ of ancient

328   seawater from 635 Ma to the present.

4. Estimation of seawater sulfate concentrations since 635 Ma

4.1 General considerations and modeling protocol

The rate and MSR-trend methods can be applied to analysis of long-term variation in seawater sulfate concentrations. Although both methods utilize measured values of $\Delta^{34}S_{sulfate-sulfide}$ as a proxy for F_{MSR}, they are quasi-independent in having different transform functions. The transform function of the rate method (Eqs. 3-4) makes use of observed rates of seawater sulfate S-isotopic variation (i.e., $\partial\delta^{34}S_{CAS}/\partial t(max)$), whereas that of the MSR-trend method (Eqs. 6-8) makes use of an empirical relationship between F_{MSR} and $[SO_4^{2-}]_{aq}$. The two methods are applicable over approximately the same range of $[SO_4^{2-}]_{SW}$ concentrations (~0.1-30 mM). However, their transform functions have different sensitivities to $[SO_4^{2-}]_{SW}$, with that of the MSR-trend method being greater as reflected in its lower slope ($m = 0.42$; Fig. 2) compared with that of the rate method ($m = 1.0$; Fig. 1). Thus, a combination of the two methods may be the most useful approach to constraining ancient seawater $[SO_4^{2-}]$. Because the rate method yields estimates of *maximum* likely $[SO_4^{2-}]_{SW}$, it should generally yield a higher estimated sulfate concentration than the MSR-trend method, which estimates the mean $[SO_4^{2-}]_{SW}$ of the time interval of interest. The pairing of these procedures is thus useful in providing both mean and maximum estimates of paleo-seawater sulfate concentrations. Combining these two methods is also useful in providing a check on the robustness of the results. For example, if the maximum estimate yielded by the rate method is less than the mean estimate yielded by the MSR-trend method, then the results should be considered unreliable.

Both the rate and MSR-trend methods require defined input variables for calculation of paleo-seawater $[SO_4^{2-}]$. For the rate method, a record of secular variation in seawater sulfate $\delta^{34}S$ is needed from which to calculate $\partial\delta^{34}S_{CAS}/\partial t$. We generated a seawater sulfate $\delta^{34}S$ record for the Phanerozoic by combining published $\delta^{34}S_{CAS}$ datasets for the Cenozoic (Paytan et al., 1998), Cretaceous (Paytan et al., 2004), and pre-Cretaceous (Kampschulte and Strauss, 2004) (Table A2; Fig. 3a). We calculated LOWESS curves for this composite record per the methodology of Song et al. (2014). LOWESS curves were generated at both a low frequency (i.e., 5-Myr steps) and a high frequency (i.e., 1-Myr steps), the latter resulting in less smoothing of the long-term $\delta^{34}S_{CAS}$ trend (Fig. 3a). The LOWESS curves were then used to calculate rates of change in seawater sulfate concentrations ($\partial\delta^{34}S_{SO4}/\partial t$) through the Phanerozoic (Fig. 3b). For both the rate and MSR-trend methods, $\Delta^{34}S_{sulfate-sulfide}$ is a defined input variable. As a proxy, we utilized the Phanerozoic $\Delta^{34}S_{CAS-PY}$ record of Wu et al. (2010). According to this record, $\Delta^{34}S_{CAS-PY}$ averaged 30±3‰ from 540 to 300 Ma, increased gradually from 30‰ to 45‰ between 300 and 270 Ma, and then fluctuated around 42±5‰ from 270 to 0 Ma (Fig. 3c).

4.2 Long-term variation in seawater sulfate concentrations

Our composite record shows that seawater sulfate $\delta^{34}S$ was heavy (~30-40‰) during the Ediacaran to Middle Cambrian, declined steeply during the Late Cambrian to Early Ordovician, and stabilized at intermediate values (~20-30‰) during the Middle Ordovician to Early

369 Devonian (Table A3; Fig. 3a). Sulfate δ^{34}S declined further during the Middle Devonian to Early
370 Mississippian, reaching a minimum of ~12-16‰ during the mid-Mississippian to end-Permian.
371 Sulfate δ^{34}S then rose sharply to ~20‰ during the Early Triassic, before declining slightly to a
372 local minimum of ~15‰ around the Jurassic-Cretaceous boundary. Sulfate δ^{34}S rose slowly
373 during the Cretaceous and early Cenozoic, increased rapidly from 17‰ to 22‰ at 40-50 Ma,
374 and then stabilized at 21-23‰ during the mid- to late Cenozoic (Fig. 3a). The low-frequency
375 LOWESS curve exhibits low rates of δ^{34}S variation, with a mean of 0.25(±0.17)‰ Myr^{-1} and a
376 maximum of ~0.8‰ Myr^{-1} (Fig. 3b). The high-frequency LOWESS curve exhibits somewhat
377 higher rates of δ^{34}S variation, with a mean of 0.40(±0.45)‰ Myr^{-1} and a maximum of ~2.5‰
378 Myr^{-1} (Fig. 3b). Both curves show exceptionally low rates of seawater sulfate δ^{34}S variation
379 during the Late Cretaceous and Cenozoic (the 'Cenozoic minimum') and the mid-Mississippian
380 to mid-Permian (the 'Late Paleozoic minimum').

381   Our reconstructions of mean and maximum seawater sulfate concentrations through
382 the Phanerozoic, based respectively on the MSR-trend and rate methods, are shown in Figure 4.
383 The mean curve suggests that $[SO_4^{2-}]_{SW}$ was low in the late Ediacaran (~1-4 mM) but rose
384 sharply in the Early Cambrian (to ~3-15 mM) and remained in that range until the Permian. A
385 long, slow rise in $[SO_4^{2-}]_{SW}$ began in the Early Permian and culminated at ~12-38 mM in the
386 Middle Triassic. Subsequently, $[SO_4^{2-}]_{SW}$ declined slightly by the mid-Cretaceous (to ~7-25 mM)
387 and then rose slightly during the Late Cretaceous to early Cenozoic (to 11-35 mM). The
388 standard deviation range for the mean curve (blue band) suggests an uncertainty of plus or
389 minus a factor of ~2× in the mean estimate, with the magnitude of the uncertainty shrinking
390 modestly from the Cambrian to the present. The modern seawater sulfate concentration of 29
391 mM falls within the standard deviation range of the mean trend (Fig. 4).

392   A maximum $[SO_4^{2-}]_{SW}$ curve can be calculated for both the low- and high-frequency
393 Phanerozoic δ^{34}S records of Figure 3a. The low- and high-frequency maximum $[SO_4^{2-}]_{SW}$ curves
394 (shown as black and red lines, respectively, in Figure 4) mirror the upward trend through the
395 Phanerozoic seen in the mean curve and, thus, are consistent with a factor of ~4× increase in
396 seawater sulfate concentrations since the Early Cambrian. Although the maximum $[SO_4^{2-}]_{SW}$
397 curves exhibit values that are mostly unrealistically large, it is worth noting that (1) these curves
398 represent the maximum possible, not the most likely, concentrations of seawater sulfate; and
399 (2) the smallest values on the maximum curves are more robust constraints on $[SO_4^{2-}]_{SW}$ than
400 the largest values. The second observation is based on the fact that the smallest values derive
401 from the largest measured rates of $\delta^{34}S_{CAS}$ variation (Fig. 3b), i.e., those rates than most closely
402 approach the theoretical maximum, whereas the largest values are associated with intervals of
403 little or no $\delta^{34}S_{CAS}$ variation. Thus, the lower envelope of maximum $[SO_4^{2-}]_{SW}$ values (dashed
404 line, Fig. 4) provides a more useful constraint on seawater sulfate concentrations than the full
405 curve. We also suggest that, although the upper limits on $[SO_4^{2-}]_{SW}$ imposed by the rate
406 method may have limited utility for assessment of Phanerozoic seawater sulfate, this method
407 may be of greater value in analyzing Archean and Proterozoic seawater sulfate concentrations,
408 which are thought to have been quite low (<1 mM; Kah et al., 2004; Canfield et al., 2007;
409 Planavsky et al., 2012).

410   The results of the rate method are dependent on several factors that influence the
411 estimation of rates of seawater sulfate $\delta^{34}S$ variation. $\partial\delta^{34}S_{SO4}/\partial t(max)$ may be overestimated
412 if there is an increase in $\delta^{34}S_{CAS}$ variance due to diagenesis or procedural artifacts during CAS
413 extraction, or it may be underestimated if there is a decrease in $\delta^{34}S_{CAS}$ variance due to
414 diagenesis or procedural data smoothing. Data smoothing is inherent in the calculation of
415 LOWESS curves (cf. Song et al., 2014), and underestimation of $\partial\delta^{34}S_{SO4}/\partial t(max)$ is thus almost
416 certain when smoothed $\delta^{34}S_{SO4}$ datasets are used as inputs. It may be responsible for the
417 absence of short-term excursions in our Phanerozoic $[SO_4^{2-}]_{SW}$ curve (Fig. 3a), since a number
418 of short (<2-Myr) intervals of strongly elevated $\partial\delta^{34}S_{SO4}/\partial t$ rates have been documented for the
419 Phanerozoic (Wortmann and Chernyavsky, 2007; Adams et al., 2010; Gill et al., 2011a,b;
420 Newton et al., 2011; Wotte et al., 2012; Owens et al., 2013; Song et al., 2014; see Section 4.3).
421 During these intervals, $\partial\delta^{34}S_{SO4}/\partial t$ ranged from 10 to >50‰ Myr^{-1} (Table A4), rates that are
422 considerably higher than peak rates for the long-term $\delta^{34}S_{CAS}$ curve (ca. 2-4‰ Myr^{-1}; Fig. 3b).
423 Because lower values for $\partial\delta^{34}S_{SO4}/\partial t(max)$ yield higher maximum estimates of $[SO_4^{2-}]$ for
424 ancient seawater (Eqs. 3-4), smoothing may account for some of the divergence between the
425 mean and maximum trends in Figure 4. The existence of such short-term episodes of seawater
426 sulfate drawdown during the Phanerozoic has been attributed to several causes, including
427 episodic massive evaporite deposition (Wortmann and Paytan, 2012) and reduced ventilation of
428 marine sediments and a consequent increase in MSR in the aftermath of mass extinction events
429 (Canfield and Farquhar, 2009).

430   Comparison of our Phanerozoic seawater sulfate concentration curve with previously
431 published estimates reveals similarities and differences (Fig. 5). Most of these records exhibit a
432 local minimum during the Jurassic or Cretaceous, although the absolute estimates of $[SO_4^{2-}]$ for
433 this minimum vary widely (~2 to 25 mM). Our higher estimates (~13-16 mM) compared to
434 those of Wortmann and Paytan (2012) (uniformly <7 mM) may be a consequence of our choice
435 of input dataset, i.e., the Phanerozoic $\Delta^{34}S_{CAS-PY}$ record of Wu et al. (2010). The latter is based
436 on a large compilative dataset that yielded a strongly time-averaged trend, which is likely to
437 have dampened variation in our $[SO_4^{2-}]_{SW}$ estimates. The various records are also in agreement
438 that seawater sulfate was elevated during the Permian-Triassic, with concentrations of ~15-30
439 mM. The records diverge prior to the Permian, however, with one model (Holser et al., 1989)
440 suggesting high values (30-50 mM) and another model (Berner, 2004) low values (<2 mM)
441 through the mid-Paleozoic. Our model indicates intermediate sulfate concentrations (5-10
442 mM) at that time (Fig. 5). The various records also show dissimilar patterns across the
443 Ediacaran-Cambrian boundary, with uniformly high values in the Holser et al. (1989) model and
444 steeply falling values in the Berner (2004) model. The results of the present study favor a steep
445 rise in seawater sulfate at this boundary. Our Phanerozoic seawater sulfate concentration
446 record, along with that of Halevy et al. (2012), is in good agreement with the available fluid-
447 inclusion data (Fig. 5) and, thus, appears generally robust, although it probably does not
448 capture short-term episodes of seawater sulfate drawdown (see Section 4.3).

449   Our reconstruction of long-term secular variation in seawater sulfate concentrations
450 shows a strong relationship to first-order Phanerozoic climate cycles (cf. Algeo et al., 2014). In
451 particular, the interval of the Late Paleozoic Ice Age, which lasted from the mid-Mississippian

452 through the mid-Permian, was characterized by a major change in the oceanic sulfate reservoir.
453 At that time, minimum values developed for both seawater sulfate $\delta^{34}S$ (~12-16‰; Fig. 3a) and
454 rates of $\delta^{34}S_{SO4}$ variation (<1‰ Myr^{-1}; Fig. 3b), accompanied by a concurrent increase in sulfate-
455 sulfide fractionation (from <30‰ to >40‰; Fig. 3c). Whether these are general features of
456 seawater sulfate during icehouse climate modes is not entirely certain. A second interval of
457 global climatic cooling and continental glaciation during the Late Cretaceous and Cenozoic also
458 shows low rates of $\delta^{34}S_{SO4}$ variation and an increase in sulfate-sulfide fractionation but, in
459 contrast to the Late Paleozoic, ^{34}S-enriched and relatively stable seawater sulfate $\delta^{34}S$ values
460 (Fig. 3). The greater stability of seawater sulfate $\delta^{34}S$ during the Cenozoic relative to the Late
461 Paleozoic may be due to a long-term increase in total seawater sulfate mass (Figs. 4-5). We
462 hypothesize that the Late Paleozoic was characterized by low rates of pyrite burial (hence,
463 lower $\delta^{34}S_{SO4}$) and a consequent increase in the mass of seawater sulfate (hence, lower
464 $\partial\delta^{34}S_{SO4}/\partial t$) (cf. Halevy et al., 2012). Low rates of pyrite burial at that time may have been due
465 to a combination of lower sea-level elevations (reducing the total shelf area available for sulfate
466 reduction; cf. Halevy et al., 2012; Algeo et al., 2014), enhanced oceanic ventilation (increasing
467 aerobic decay of organic matter), and increased burial of organic matter in low-sulfate
468 freshwater settings, which was linked to the spread of terrestrial floras (DiMichele and Hook,
469 1992).

470

471 ## 4.3 High-frequency variation in seawater sulfate during the Neoproterozoic and
472 Phanerozoic

473 We applied the rate and MSR-trend methods to an analysis of short-term variation in $[SO_4^{2-}]_{SW}$
474 during selected intervals of the Neoproterozoic and Phanerozoic for which high-resolution
475 $\delta^{34}S_{CAS}$ studies are available. For the Neoproterozoic, recent studies have provided S-isotope
476 records from a number of sites globally as well as improved radiometric geochronologic
477 constraints that are needed for the rate method. Based on these studies, we have estimated
478 $\partial\delta^{34}S_{SO4}/\partial t(max)$ for 10 late Neoproterozoic units (Table A4; Fig. 6). Radiometric studies of the
479 Doushantuo Formation in South China (Halverson et al., 2005; Zhang et al., 2005, 2008)
480 provided key ages from which we calculated $\partial\delta^{34}S_{CAS}/\partial t(max)$ of 5‰ Myr^{-1} at ~636-633 Ma and
481 1.3‰ Myr^{-1} at ~568-551 Ma (McFadden et al., 2008; Li et al., 2010). The Neoproterozoic
482 succession of Sonora, Mexico yielded $\partial\delta^{34}S_{CAS}/\partial t(max)$ estimates of 6‰ Myr^{-1} and 4‰ Myr^{-1}
483 (Loyd et al., 2012, 2013). The latest Neoproterozic Zarls Formation (Nama Group) in Namibia
484 and upper Huqf Supergroup in Oman yielded $\partial\delta^{34}S_{CAS}/\partial t(max)$ estimates of 20‰ Myr^{-1} and
485 40‰ Myr^{-1}, respectively, at 549-547 Ma (Fike and Grotzinger, 2008; Ries et al., 2009). The rate
486 method yielded $[SO_4^{2-}]_{SW}$ estimates ranging from <0.1 to >100 mM, with most between ~1 and
487 10 mM (Table A4). The MSR-trend method yielded $[SO_4^{2-}]_{SW}$ estimates ranging from <0.1 to 70
488 mM, with most between ~1 and 16 mM. Many units exhibit combinations of $\partial\delta^{34}S_{CAS}/\partial t(max)$
489 and $\Delta^{34}S_{CAS-PY}$ values that plot close to or slightly below the MSR trend (Fig. 6), yielding
490 $[SO_4^{2-}]_{SW}$ estimates for the MSR-trend method that are equal to or somewhat smaller than the
491 rate-based estimates. This pattern conforms to our expectation that the rate method yields
492 maximum estimates of $[SO_4^{2-}]_{SW}$. The only potentially anomalous result is for the upper Huqf

493 Supergroup, which yielded a MSR-trend estimate (12-45 mM) that is larger than the rate-
494 method estimate (1.5-8 mM; Table A4).

495 　　　　We also analyzed $[SO_4^{2-}]_{SW}$ for a set of 8 units of Cambrian age. These units yielded
496 $\partial\delta^{34}S_{CAS}/\partial t(max)$ of 7 to 23‰ Myr^{-1} for the Early Cambrian, 9 to 20‰ Myr^{-1} for the Early-Middle
497 Cambrian boundary (EMCB), and 8 to 20‰ Myr^{-1} for the Late Cambrian SPICE (Table A4; Fig. 7).
498 These ranges are sufficiently similar that they suggest a limited range of seawater $[SO_4^{2-}]$
499 variation during the Cambrian. The rate method yielded $[SO_4^{2-}]_{SW}$ estimates ranging from <0.1
500 to 18 mM, with most between ~1 and 6 mM. The MSR-trend method yielded $[SO_4^{2-}]_{SW}$
501 estimates ranging from <0.1 to 40 mM, with most between ~1 and 8 mM. The two methods
502 thus yielded similar estimates of seawater sulfate concentrations, implying that the results are
503 reasonably robust and that the rate method is not yielding unrealistically large values. All
504 Cambrian units show sulfate-sulfide fractionations smaller than the Paleozoic mean of 30±5
505 (Wu et al., 2010), resulting in lower $[SO_4^{2-}]_{SW}$ estimates than for the long-term record (Fig. 4).
506 Once again, most units exhibit combinations of $\partial\delta^{34}S_{CAS}/\partial t(max)$ and $\Delta^{34}S_{CAS-PY}$ values that plot
507 close to or slightly below the MSR trend (Fig. 7). However, two units (the SPICE events in
508 Australia and Nevada) yield MSR-trend estimates that are larger than their rate-method
509 estimates. The reasons for these potentially anomalous results will be considered below.

510 　　　　Finally, we analyzed a set of 8 Mesozoic units, ranging in age from the Early Triassic to
511 the late Middle Cretaceous (Table A4; Fig. 8). These units show $\partial\delta^{34}S_{CAS}/\partial t(max)$ of 6 to 60‰
512 Myr^{-1}, with the highest rates during the Early Triassic and Early Jurassic. The rate method
513 yielded $[SO_4^{2-}]_{SW}$ estimates ranging from 1.1 to 120 mM, with most between ~3 and 20 mM.
514 The MSR-trend method yielded $[SO_4^{2-}]_{SW}$ estimates ranging from 1 to 110 mM, with most
515 between ~30 and 100 mM (Table A4). In contrast to the late Neoproterozoic and Cambrian,
516 many Mesozoic units exhibit a narrow spread of $\Delta^{34}S_{CAS-PY}$ values that conform with the mean
517 sulfate-sulfide fractionation for the Mesozoic-Cenozoic (Wu et al., 2010; Fig. 8) and that are
518 within the range for modern marine systems (~30-60‰; Table A1). As a consequence, many
519 Mesozoic units exhibit the anomalous pattern of having MSR-trend estimates that are larger
520 than their rate-method estimates.

521 　　　　Ideally, the rate and MSR-trend methods will yield similar $[SO_4^{2-}]_{SW}$ estimates, providing
522 support for the correctness of the results, and a majority of the paleomarine units considered in
523 this study follow this pattern. However, a subset of the study units show differences that fall
524 into two categories: (1) Type I deviation: rate method estimates >> MSR-trend estimates (lower
525 right field, Fig. 9), and (2) Type II deviation: MSR-trend estimates >> rate method estimates
526 (upper left field, Fig. 9). Such deviations may provide insights into underlying controls on
527 seawater sulfate concentrations. The most likely explanation for the Type I deviations is that
528 the measured $\partial\delta^{34}S_{CAS}/\partial t(max)$ for a given unit is much less than its theoretical maximum. This
529 situation can develop whenever the marine sulfur cycle is in equilibrium (i.e., source and sink
530 fluxes in balance), reflecting persistently stable environmental conditions. In this case, the rate-
531 method estimate of $[SO_4^{2-}]_{SW}$ would have little relationship to actual $[SO_4^{2-}]_{SW}$, although the
532 MSR-trend estimate may still be a good proxy for $[SO_4^{2-}]_{SW}$. Surprisingly, very few of the
533 analyzed units (Table A4) show Type I deviations, perhaps because the most heavily scrutinized
534 ancient geologic epochs are those with unstable environments.

535   Type II deviations, in which $\partial\delta^{34}S_{CAS}/\partial t$(max) is anomalously high, are more common,

536   being present in three units of late Neoproterozoic and Cambrian age (Figs. 6-7) and 7 out of 8

537   units of Mesozoic age (Fig. 8). Several factors might potentially produce this pattern. First,

538    $\partial\delta^{34}S_{CAS}/\partial t$(max) may have been overestimated owing to inadequate geochronologic

539   constraints, diagenetic artifacts, or analytical uncertainties in measuring $\delta^{34}S_{CAS}$. However, the

540   fact that Type II deviations are more common among Mesozoic units (Fig. 8), which are

541   generally better dated and less diagenetically altered than older units (Figs. 6-7), suggests that

542   such problems are relatively uncommon and unlikely to be responsible for most such

543   anomalies. Second, the measured $\Delta^{34}S_{CAS-PY}$ for a given paleomarine unit may be

544   unrepresentative, perhaps because of unusually large MSR fractionation (cf. Habicht et al.,

545   2002; Canfield et al., 2010). This explanation may be applicable, for example, to Pleistocene

546   Mediterranean sapropels (Scheiderich et al., 2010), which exhibit unusually large $\Delta^{34}S_{CAS-PY}$

547   values (60±5‰; Fig. 8). However, none of the anomalous units of late Neoproterozoic,

548   Cambrian, or Mesozoic age exhibits a $\Delta^{34}S_{CAS-PY}$ larger than the typical modern range of ~30-

549   60‰, so elevated sulfate-sulfide fractionation is unlikely as a general explanation. We are

550   therefore inclined to regard most Type II deviations as products of local depositional conditions

551   and to seek an environmentally based mechanism to account for them.

552   A possible environmental explanation for Type II deviations is sulfate reduction within a

553   restricted-marine basin. In this case, $\Delta^{34}S_{CAS-PY}$ is controlled by seawater $[SO_4^{2-}]$, which may be

554   identical (or nearly so) to that in the global ocean. However, the total mass of sulfate in the

555   restricted-marine basin will be much less than that in the global ocean, allowing a more rapid

556   evolution of seawater sulfate $\delta^{34}S$ in response to oceanographic perturbations. We hypothesize

557   that most of the Type II deviations in our study units are the product of MSR within semi-

558   restricted marine basins. For example, the Neoproterozoic Ara Group (Huqf Supergroup) of

559   Oman was deposited in a fault-bounded basin in which massive evaporite deposits accumulated

560   (Fike and Grotzinger, 2008). Also, most of the Mesozoic units showing Type II deviations are

561   known to have been deposited in basins that were subject to a degree of watermass restriction.

562   The Triassic-Jurassic European epicontinental sea was broad, shallow, and laced with local

563   tectonic grabens with restricted deepwater circulation (Röhl et al., 2001; Berra et al., 2010).

564   The Early Cretaceous South Atlantic was only weakly connected to the global ocean during

565   deposition of Aptian sediments (Wortmann and Chernyavsky, 2007), and restriction of the

566   Atlantic Ocean continued at least through deposition of organic-rich facies at the Cenomanian-

567   Turonian boundary (Owens et al., 2013). The Cretaceous Western Interior Seaway was almost

568   certainly semi-restricted throughout its existence (Adams et al., 2010). The only Mesozoic unit

569   not to show a Type II deviation, the Middle Triassic Bravaisberget Formation of Spitsbergen

570   (Karcz, 2010; Fig. 8), was deposited in the largely unrestricted Boreal Ocean. These examples

571   serve to illustrate the need to understand the hydrography of paleomarine basins in applying

572   the rate method of estimating paleoseawater sulfate concentrations.

573   Comparison of the $[SO_4^{2-}]_{SW}$ estimates for individual Neoproterozoic and Phanerozoic

574   units shown in Figures 6-8 with the long-term $[SO_4^{2-}]_{SW}$ curve in Figure 4 provides additional

575   insights regarding secular variation in seawater sulfate inventories. With the exception of the

576   Middle Triassic Bravaisberget Formation, all Mesozoic units exhibit MSR-trend estimates that

577   overlap the long-term trend but rate estimates that fall below it (Fig. 10). As discussed above,

578   we infer that this pattern reflects anomalously high measured $\partial\delta^{34}S_{CAS}/\partial t(max)$ values as a

579   consequence of rapid evolution of seawater sulfate $\delta^{34}S$ within semi-restricted marine basins of

580   the proto-Atlantic and western Tethys oceans. Cambrian units exhibit a wide range of $[SO_4^{2-}]_{SW}$

581   estimates, although a cluster of results falls just below the long-term trend, with many

582   estimates between 1 and 5 mM (Fig. 10). We infer that either our long-term record (Fig. 4)

583   overestimates $[SO_4^{2-}]_{SW}$ for the Cambrian, or the studied units are biased toward low $[SO_4^{2-}]_{SW}$.

584   Late Neoproterozoic units exhibit an even wider range of $[SO_4^{2-}]_{SW}$ estimates than Cambrian

585   units and lack any apparent clustering (Fig. 10). However, all but one of these units yield similar

586     $[SO_4^{2-}]_{SW}$ estimates for the MSR-trend and rate methods (Fig. 6), suggesting that the estimates

587   are robust. We infer that the late Neoproterozoic (635-542 Ma) was characterized by a highly

588   unstable marine sulfur cycle, as a consequence of which seawater sulfate concentrations varied

589   tremendously. This inference is supported by some earlier studies (Li et al., 2010; Loyd et al.,

590   2012, 2013), although other studies have inferred low (Hurtgen et al., 2002, 2005, 2006; Ries et

591   al., 2009) or monotonically rising sulfate concentrations (Halverson and Hurtgen, 2007) during

592   this interval.

593

594   **5 Conclusions**

595   The rate and MSR-trend methods developed in this study for quantifying paleo-seawater

596   sulfate concentrations are complementary and quasi-independent, providing estimates of

597   maximum and mean $[SO_4^{2-}]_{SW}$, respectively, for a paleomarine unit of interest. Both techniques

598   make use of $\Delta^{34}S_{CAS-PY}$, i.e., the isotopic fractionation associated with microbial sulfate

599   reduction (MSR). The rate method evaluates $[SO_4^{2-}]_{SW}$ as a function of $\partial\delta^{34}S_{CAS}/\partial t(max)$, i.e.,

600   the maximum observed rate of change in seawater sulfate, whereas the MSR-trend method

601   makes use of an empirical relationship between MSR fractionation and aqueous sulfate

602   concentrations. The significance of our quantitative approach is that estimates of paleo-

603   seawater $[SO_4^{2-}]$ can be derived from two readily measurable sedimentary parameters: $\Delta^{34}S_{CAS-}$

604     $_{PY}$ and $\delta^{34}S_{CAS}/\partial t(max)$. Based on these methods, an analysis of long-term variation since 635

605   Ma suggests that $[SO_4^{2-}]_{SW}$ was low during the late Neoproterozoic (<5 mM), rose sharply

606   across the Ediacaran/Cambrian boundary (to ~5-10 mM), and rose again during the Permian to

607   near-modern levels (~10-30 mM). However, high-resolution $\delta^{34}S_{CAS}$ studies provide evidence of

608   episodic high-frequency (<~2-Myr) events during which seawater sulfate concentrations were

609   drawn down in response to massive evaporite deposition, reduced sediment ventilation and

610   increased pyrite burial in the aftermath of mass extinctions, or other factors. The techniques

611   developed in this study for quantitative analysis of paleo-seawater $[SO_4^{2-}]$ should be applicable

612   to marine units of any age provided that (1) MSR fractionation has been a conservative process

613   through time (i.e., the dominant pathways of sulfur metabolism have not changed greatly), and

614   (2) sufficient time control exists for estimation of rates of $\delta^{34}S_{CAS}$ variation. As more S-isotopic

615   studies of cogenetic sulfate and sulfide become available, it should ultimately be possible to

616   reconstruct variation in seawater sulfate concentrations throughout Earth history.

617

618   Author Contributions

619   TJA developed the project concept and modeling methodology, GML, HYS, TWL, and DEC
620   provided isotopic data, and all authors assisted in drafting the manuscript.

621

Acknowledgments

627

Appendix A: Data tables

629   The primary sulfur isotopic data and model output for this study are given in Tables A1 to A4.

630

631   Table A1. MSR fractionation data for modern aqueous systems

632

633   Table A2. Phanerozoic $\delta^{34}S_{CAS}$ data

634

635   Table A3. Modeled Phanerozoic seawater sulfate $\delta^{34}S$ curve

636

637   Table A4. Analysis of high-frequency seawater sulfate variation

638

Appendix B: Extended discussion

B1 Relationship of rate of seawater sulfate change to sulfate residence time

641   The maximum possible rate of change in seawater sulfate $\delta^{34}S$ (i.e., $\partial\delta^{34}S_{SO4}/\partial t(max)$) is
642   inversely proportional to the residence time of sulfate in seawater (τ). The exact quantitative
643   form of this relationship can be derived from Equation 2 of Algeo et al. (2014), reorganization of
644   which yields:

645        $$M_{SW} / F_{PY} = k_1 \times \Delta^{34}S_{CAS-PY} / \partial\delta^{34}S_{CAS}/\partial t(max) \qquad (B1)$$

646   The residence time of sulfur in seawater is equal to the mass of seawater sulfate divided by the
647   total sink flux, i.e., the reduced sulfur flux (F_{PY}) plus the oxidized sulfur flux (F_{EVAP}):

648        $$\tau = M_{SW} / (F_{PY} + F_{EVAP}) \qquad (B2)$$

649 Letting ϕ_{PY} be the fraction of the total S flux represented by pyrite burial (i.e., F_{PY} / (F_{PY} + F_{EVAP})),
650 then:

651 $\tau \times \phi_{PY}^{-1} = M_{SW} / F_{PY}$ (B3)

652 And substitution into Equation B1 yields:

653 $\tau \times \phi_{PY}^{-1} = k_1 \times \Delta^{34}S_{CAS-PY} / \partial\delta^{34}S_{CAS}/\partial t(max)$
654 (B4)

655 This equation quantifies the inverse proportionality between the maximum rate of change of
656 seawater sulfate $\delta^{34}S$ and the residence time of sulfur in seawater.

657

658 ## B2 Effects of $[SO_4^{2-}]_{SW}$-dependent pyrite burial fluxes on $[SO_4^{2-}]_{SW}$ estimates

659 Although we made use of fixed estimates of the pyrite burial flux (F_{PY}), i.e., 4×10^{13} g yr^{-1}
660 for oxic oceans and 10×10^{13} g yr^{-1} for anoxic oceans, it is possible that F_{PY} is dependent on
661 $[SO_4^{2-}]_{SW}$. Wortmann and Chernyavsky (2007) inferred a non-linear positive relationship of F_{PY}
662 with $[SO_4^{2-}]_{SW}$ (their figure 4). We explored the effects of varying pyrite burial fluxes on
663 seawater sulfate estimates as follows. Equations 2-3 have four variables: $[SO_4^{2-}]_{SW}$ (or M_{SW},
664 since these are inter-convertible via Equation 4), F_{PY}, $\Delta^{34}S_{CAS-PY}$, and $\partial\delta^{34}S_{SO4}/\partial t$. However,
665 $\Delta^{34}S_{CAS-PY}$ can be modeled as a function of $[SO_4^{2-}]_{SW}$ (i.e., the MSR trend of Figure 2 and
666 Equation 6), reducing the number of potentially independent variables to three (we state
667 "potentially independent" as there may in fact be some dependency among these variables).
668 Now it is possible to explore the effects of simultaneous variations in $[SO_4^{2-}]_{SW}$ and F_{PY} on
669 $\partial\delta^{34}S_{SO4}/\partial t(max)$ via a modified form of Equation 2:

670

671 $\partial\delta^{34}S_{CAS}/\partial t(max) = k_1 \times k_2 \times F_{PY} \times \exp(\log[SO_4^{2-}]_{SW} * 0.42 + 1.10) / [SO_4^{2-}]_{SW}$ (B5)

672

673 The three modeled parameters exhibit log-linear relationships, with larger $\partial\delta^{34}S_{CAS}/\partial t(max)$
674 associated with larger $[SO_4^{2-}]_{SW}$ and F_{PY} (Fig. B1). $\partial\delta^{34}S_{CAS}/\partial t(max)$ scales linearly with F_{PY}, so
675 uncertainty in the latter parameter is directly mirrored in the former parameter. The range of
676 F_{PY} used in our study (i.e., 4-10 $\times 10^{13}$ g yr^{-1}) is consistent with variation in $\partial\delta^{34}S_{CAS}/\partial t(max)$
677 from ~1 to 100 ‰ Myr^{-1}. The F_{PY}-$[SO_4^{2-}]_{SW}$ relationship of Wortmann and Chernyavsky (2007,
678 their figure 4; red curve, Fig. B1), if correct, indicates that variation in $\partial\delta^{34}S_{CAS}/\partial t(max)$ cannot
679 exceed ~3 ‰ Myr^{-1} under any set of conditions.

680 We tested the influence of sulfate-dependent pyrite burial fluxes on seawater sulfate
681 concentration estimates by applying the relationship of Wortmann and Chernyavsky (2007) to
682 our rate-method calculations. Their relationship can be reduced to a logarithmic expression:

683

684 $F_{PY} = 0.7681 \times \ln([SO_4^{2-}]_{SW}) + 1.405$ (B6)

685

686   where F_{PY} is in units of 10^{13} g yr^{-1} (rather than in mol yr^{-1}, as in their paper) and [SO_4^{2-}]$_{SW}$ is in
687   units of mM. This expression yielded a r^2 of 0.98 in relation to Wortmann and Chernyavsky's
688   curve (their figure 4). In making use of sulfate-dependent pyrite burial fluxes for calculation of
689   seawater sulfate concentration estimates, Equations 3 and 4 must be reorganized as follows:

690

691   [SO_4^{2-}]$_{SW}$(max) / F_{PY} = $k_1 \times k_2 \times \Delta^{34}S_{CAS-PY} / \partial\delta^{34}S_{CAS}/\partial t$(max)   (B7)

692

693   Although Equation B7 has two unknowns, i.e., [SO_4^{2-}]$_{SW}$(max) and F_{PY}, it can be solved because
694   F_{PY} is a function of [SO_4^{2-}]$_{SW}$ in figure 4 of Wortmann and Chernyavsky (2007). The empirical
695   relationship between [SO_4^{2-}]$_{SW}$ and [SO_4^{2-}]$_{SW}$(max) / F_{PY} is given by the polynomial equation:

696

697   [SO_4^{2-}]$_{SW}$(max) / F_{PY} = -0.0018([SO_4^{2-}]$_{SW}$)^2 + 0.2842([SO_4^{2-}]$_{SW}$) + 0.4651   (B8)

698

699   With substitution and reorganization, Equations B7 and B8 yield:

700

701   0 = -0.0018([SO_4^{2-}]$_{SW}$)^2 + 0.2842([SO_4^{2-}]$_{SW}$) + (0.4651 − $k_1 \times k_2 \times \Delta^{34}S_{CAS-PY}/[\partial\delta^{34}S_{CAS}/\partial t$(max)])   (B9)

702

703   This second-order polynomial equation can now be solved for [SO_4^{2-}]$_{SW}$ using the quadratic
704   solution, after which F_{PY} can be calculated from Equation B6.

705   Using Equation B9, we calculated [SO_4^{2-}]$_{SW}$ on the basis of $\partial\delta^{34}S_{CAS}/\partial t$(max) and $\Delta^{34}S_{CAS-}$
706   $_{PY}$. These relationships are plotted as variation in $\partial\delta^{34}S_{CAS}/\partial t$(max) as a function of [$SO_4^{2-}$]$_{SW}$
707   and $\Delta^{34}S_{CAS-PY}$ (Fig. B2; cf. Figure 1). At high [SO_4^{2-}]$_{SW}$, the two sets of $\partial\delta^{34}S_{CAS}/\partial t$(max) curves
708   are nearly co-linear, which is because the value of F_{PY} in figure 4 of Wortmann and Chernyavsky
709   (2007) for [SO_4^{2-}]$_{SW}$ >10 mM is nearly invariant and similar to the flux that we used for oxic
710   marine environments (i.e., 4 × 10^{13} g yr^{-1}). In contrast, the two sets of curves diverge sharply at
711   [SO_4^{2-}]$_{SW}$ <1 mM, which is a consequence of the much lower F_{PY} values associated with low
712   seawater sulfate concentrations in the Wortmann and Chernyavsky curve.

713   The $\partial\delta^{34}S_{CAS}/\partial t$(max) curves based on the sulfate-dependent pyrite fluxes of Wortmann
714   and Chernyavsky (2007) require comment. First, the MSR trend (Figure 2) corresponds almost
715   entirely to a limited range of $\partial\delta^{34}S_{CAS}/\partial t$(max) values (i.e., 2 to 4; Fig. B2). This suggests that
716   there ought to be quite limited variation in $\partial\delta^{34}S_{CAS}/\partial t$(max) over a wide range of seawater
717   sulfate concentrations in nature. Second, many combinations of the two sediment parameters
718   that can be measured (i.e., $\Delta^{34}S_{CAS-PY}$ and $\partial\delta^{34}S_{CAS}/\partial t$(max)) cannot yield a [$SO_4^{2-}$]$_{SW}$ estimate.
719   For example, no [SO_4^{2-}]$_{SW}$ estimate is possible for $\Delta^{34}S_{CAS-PY}$ of 7‰ in combination with any
720   $\partial\delta^{34}S_{CAS}/\partial t$(max) value that is larger than ~4 (Fig. B2). This situation exists because high rates
721   of variation in seawater sulfate $\delta^{34}S$ are not possible where the pyrite burial flux is sharply

722   curtailed by $[SO_4^{2-}]_{SW}$-dependency (as in figure 4 of Wortmann and Chernyavsky, 2007).
723   However, many paleomarine units exhibit $\partial\delta^{34}S_{CAS}/\partial t(max)$ values outside the narrow range
724   permitted by the Wortmann and Chernyavsky (2007) relationship (see Table A4 and Figures 6-
725   8). If the Wortmann and Chernyavsky (2007) parameterization of the F_{PY}-$[SO_4^{2-}]_{SW}$ relationship
726   is correct, then one must conclude either that all of these published higher rates are products
727   of uncertain geochronologic dating, diagenetic artifacts, or sample processing and analytical
728   problems. On the other hand, the use of fixed values for F_{PY} in our rate-method calculations
729   (Eqs. 2-4) yields estimates of $[SO_4^{2-}]_{SW}$ that are—for the most part—consistent with estimates
730   of $[SO_4^{2-}]_{SW}$ based on the MSR-trend method (Section 2.2; see Figures 6-8 for examples). We
731   acknowledge that some form of sulfate-dependency of pyrite burial fluxes may exist but
732   suggest that it may differ from the relationship given by Wortmann and Chernyavsky (2007).

733

B3 Sources of sulfide $\delta^{34}S$ data

735   Although all sulfate $\delta^{34}S$ data used in the calculation of $\Delta^{34}S_{sulfate-sulfide}$ values in Figure 2
736   are based on aqueous SO_4^{2-} measurements, we used sulfide $\delta^{34}S$ data from multiple sources:
737   pyrite, sediment acid-volatile sulfur (AVS), sediment total reduced sulfur (TRS), and aqueous
738   H_2S (Table A1). We have constructed a version of Figure 2 that shows the different sulfide
739   phases, and we calculated separate regressions for each phase (Fig. B3). The following points
740   should be noted about this figure. First, each of the four phases yields a statistically significant
741   regression (r = 0.81-0.92; $p(\alpha)$ <0.05; Table B1). Second, the four phases have similar regression
742   slopes although slightly variable y-intercepts. For this reason, TRS and AVS yield $\Delta^{34}S_{CAS-PY}$
743   values that are, on average, slightly larger for a given $[SO_4^{2-}]_{SW}$ than pyrite and aqueous H_2S.
744   Third, the four regression lines generally converge at higher $[SO_4^{2-}]_{SW}$, and the largest
745   differences occur at low $[SO_4^{2-}]_{SW}$, where data is sparser.

746   One point that bears reflection is that estimates of paleoseawater $[SO_4^{2-}]_{SW}$ are based
747   not on aqueous sulfide $\delta^{34}S$, which cannot be measured for paleomarine systems, but on
748   mineral sulfide (generally pyrite) $\delta^{34}S$. Therefore, the critical relationship for establishing a
749   viable MSR-trend proxy for $[SO_4^{2-}]_{SW}$ is that between sulfate $\delta^{34}S$ and pyrite $\delta^{34}S$. Although we
750   could have used the pyrite $\delta^{34}S$ data alone, we opted to include other sulfide phases to produce
751   a larger sulfide $\delta^{34}S$ dataset, especially one containing more data at low $[SO_4^{2-}]_{SW}$, with the goal
752   of generating a stable relationship over a wider range of $[SO_4^{2-}]_{SW}$ values. Whether there are
753   real differences in the regression relationships among these four sulfide phases is an issue that
754   will require further inquiry. These sulfide phases yield similar relationships between $\Delta^{34}S_{sulfate-}$
755    $_{sulfide}$ and $[SO_4^{2-}]_{SW}$ that, based on the available data, are statistically indistinguishable (Fig. B3).

756

757   Table B1. Regression statistics for reduced sulfur phases (see Figure B3)

Sulfur phase	n	r	m	b	p(α)
Pyrite	48	0.92	0.46	-0.35	<0.01
Sediment AVS	6	0.81	0.42	-0.06	<0.05

Sediment TRS	11	0.89	0.33	0.20	<0.01
Aqueous H_2S	16	0.84	0.44	-0.20	<0.01

758

759

760 Figure B1. Relationship of $\partial\delta^{34}S_{CAS}/\partial t$(max) to F_{PY} and $[SO_4^{2-}]_{SW}$, with $\Delta^{34}S_{CAS-PY}$ estimated as a
761 function of $[SO_4^{2-}]_{SW}$ (Figure 2, Equation 6). The dashed horizontal lines represent the pyrite
762 burial fluxes used in this study for oxic and anoxic paleomarine systems, i.e., 4×10^{13} g yr^{-1} and
763 10×10^{13} g yr^{-1}, respectively. The red line represents the $[SO_4^{2-}]_{SW}$-dependency of the pyrite
764 burial flux as given by Wortmann and Chernyavsky (2007, their figure 4). Note that according to
765 the latter relationship, $\partial\delta^{34}S_{CAS}/\partial t$(max) values cannot exceed ~3 ‰ Myr^{-1} under any set of
766 conditions.

767

768 Figure B2. $\partial\delta^{34}S_{CAS}/\partial t$(max) values calculated using fixed pyrite burial fluxes (blue diagonal
769 lines; cf. Figure 1) and the sulfate-dependent pyrite burial fluxes of Wortmann and Chernyavsky
770 (2007; red curves). Note that, for the latter curves, many combinations of the two measured
771 sediment parameters ($\Delta^{34}S_{CAS-PY}$ and $\partial\delta^{34}S_{CAS}/\partial t$(max)) cannot yield a $[SO_4^{2-}]_{SW}$ estimate.
772 Shown for reference is the MSR trend of Figure 2.

773

774 Figure B3. Replotted MSR trend data (from Figure 2, Table A1) as a function of sulfide $\delta^{34}S$
775 source (symbols as given in legend). Separate regressions for the four different sulfide phases
776 (dashed lines) show small differences in slopes and y-intercepts (Table B1), although the
777 regression lines are statistically indistinguishable.

778

References

Adams, D. D., Hurtgen, M. T. and Sageman, B. B.: Volcanic triggering of a biogeochemical cascade during Oceanic Anoxic Event 2. Nat. Geosci., 3, 201-204, 2010.

Algeo, T. J., Meyers, P. A., Robinson, R. S., Rowe, H. and Jiang, G. Q.: Icehouse-greenhouse variations in marine denitrification. Biogeosciences, 11, 1273-1295, 2014.

Asmussen, G. and Strauch, G.: Sulfate reduction in a lake and the groundwater of a former lignite mining area studied by stable sulfur and carbon isotopes. Water Air Soil Poll., 108, 271-284, 1998.

Bates, A. L., Spiker, E. C., Hatcher, P. G., Stout, S. A. and Weintraub, V. C.: Sulfur geochemistry of organic-rich sediments from Mud Lake, Florida, U.S.A. Chem. Geol., 121, 245-262, 1995.

Bates, A. L., Spiker, E. C. and Holmes, C. W.: Speciation and isotopic composition of sedimentary sulfur in the Everglades, Florida, USA. Chem. Geol., 146, 155-170, 1998.

Bates, A. L., Spiker, E. C., Orem, W. H. and Burnett, W.C.: Speciation and isotopic composition of sulfur in sediments from Jellyfish Lake, Palau. Chem. Geol., 106, 63-76, 1993.

Bekker, A., Holland, H. D., Wang, P. L., Rumble, D., III, Stein, H. J., Hannah, J. L., Coetzee, L. L. and Beukes, N. J.: Dating the rise of atmospheric oxygen. Nature, 427, 117-120, 2004.

Bergman, N. M., Lenton, T. M. and Watson, A. J.: COPSE: a new model of biogeochemical cycling over Phanerozoic time. Am. J. Sci., 397-437, 2004.

Berner, R. A.: A model for calcium, magnesium and sulfate in seawater over Phanerozoic time. Am. J. Sci., 304, 438-453, 2004.

Berner, Z. A., Puchelt, H., Nöltner, T. and Kramar, U.: Pyrite geochemistry in the Toarcian Posidonia Shale of southwest Germany: evidence for contrasting trace-element patterns of diagenetic and syngenetic pyrites. Sedimentology, 60, 548-573, 2013.

Berra, F., Jadoul, F. and Anelli, A.: Environmental control on the end of the Dolomia Principale/Hauptdolomit depositional system in the central Alps: coupling sea-level and climate changes. Palaeogeogr. Palaeoclimatol. Palaeoecol., 290, 138-150, 2010.

Böttcher, M. E., Voss, M., Schulz-Bull, D., Schneider, R., Leipe, T. and Knöller, K.: Environmental changes in the Pearl River Estuary (China) as reflected by light stable isotopes and organic contaminants. J. Mar. Syst., 82, S43-S53, 2010.

Bottrell, S. H. and Newton, R. J.: Reconstruction of changes in global sulfur cycling from marine sulfate isotopes. Earth-Sci. Rev., 75, 59-83, 2006.

Bradley, A. S., Leavitt, W. D. and Johnston, D. T.: Revisiting the dissimilatory sulfate reduction pathway. Geobiology, 9, 446-457, 2011.

Brennan, S. T., Lowenstein, T. K. and Horita, J.: Seawater chemistry and the advent of biocalcification. Geology, 32, 473-476, 2004.

Brüchert, V.: Physiological and ecological aspects of sulfur isotope fractionation during bacterial sulfate reduction, in: Amend, J. P., Edwards, K. J. and Lyons, T. W. (Eds.), Sulfur Biogeochemistry—Past and Present, Geol. Soc. Am. Spec. Pap., 379, 1-16, 2004.

Brüchert, V. and Pratt, L. M.: Contemporaneous early diagenetic formation of organic and inorganic sulfur in estuarine sediments from St. Andrew Bay, Florida, USA. Geochim. Cosmochim. Acta, 60, 2325-2332, 1996.

821   Brüchert, V. and Pratt, L. M.: Stable sulfur isotopic evidence fro historical changes of sulfur
822   cycling in estuarine sediments from northern Florida. Aquat. Geochem., 5, 249-268,
823   1999.
824   Brüchert, V., Knoblauch, C. and Jørgensen, B. B.: Microbial controls on the stable sulfur isotope
825   fractionation during bacterial sulfate reduction in Arctic sediments. Geochim.
826   Cosmochim. Acta, 65, 753-766, 2001.
827   Brunner, B. and Bernasconi, S. M.: A revised isotope fractionation model for dissimilatory
828   sulfate reduction in sulfate-reducing bacteria. Geochim. Cosmochim. Acta, 69, 4759-
829   4771, 2005.
830   Canfield, D. E.: A new model for Proterozoic ocean chemistry. Nature, 396, 450-453, 1998.
831   Canfield, D. E.: Isotope fractionation by natural populations of sulfate-reducing bacteria.
832   Geochim. Cosmochim. Acta, 65, 1117-1124, 2001.
833   Canfield, D. E.: The evolution of the Earth surface sulfur reservoir. Am. J. Sci., 304, 839-861,
834   2004.
835   Canfield, D. E. and Farquhar, J.: Animal evolution, bioturbation, and the sulfate concentration of
836   the oceans. Proc. Nat. Acad. Sci. (U.S.A.), 106, 8123-8127, 2009.
837   Canfield, D. E. and Raiswell, R.: The evolution of the sulfur cycle. Am. J. Sci., 299, 697-723, 1999.
838   Canfield, D. E. and Thamdrup, B. T.: The production of ^{34}S-depleted sulfide during
839   disproportionation of elemental sulfur. Science, 266, 1973-1975, 1994.
840   Canfield, D. E., Raiswell, R. and Bottrell, S.: The reactivity of sedimentary iron minerals toward
841   sulfide. Am. J. Sci., 292, 659-683, 1992.
842   Canfield, D. E., Olesen, C. A. and Cox, R. P.: Temperature and its control of isotope fractionation
843   by a sulfate-reducing bacterium. Geochim. Cosmochim. Acta, 70, 548-561, 2006.
844   Canfield, D. E., Poulton, S. W. and Narbonne, G. M.: Late-Neoproterozoic deep-ocean
845   oxygenation and the rise of animal life. Science, 315, 92-95, 2007.
846   Canfield, D. E., Farquhar, J. and Zerkle, A. L.: High isotope fractionations during sulfate
847   reduction in a low-sulfate euxinic ocean analog. Geology, 38, 415-418, 2010.
848   Chambers, L. A., Trudinger, P. A., Smith, J. W. and Burns, M. S.: Fractionation of sulfur isotopes
849   by continuous cultures of *Desulfovibrio desulfuricans*. Can. J. Microbiol., 21, 1602-1607,
850   1975.
851   Chanton, J. P. and Lewis, F. G.: Plankton and dissolved inorganic carbon isotopic composition in
852   a river-dominated estuary: Apalachicola Bay, Florida. Estuaries, 22, 575-583, 1999.
853   Detmers, J., Brüchert, V., Habicht, K. S. and Kuever, J.: Diversity of sulfur isotope fractionations
854   by sulfate-reducing prokaryotes. Appl. Environ. Microbiol., 67, 888-894, 2001.
855   DiMichele, W. A. and Hook, R. W.: Paleozoic terrestrial ecosystems, in: Behrensmeyer, A. K., et
856   al. (Eds.), Terrestrial Ecosystems through Time, The University of Chicago Press, 205-325,
857   1992.
858   Doi, H., Kikuchi, E., Mizota, C., Satoh, N., Shikano, S., Yurlova, N., Yadrenkina, E. and Zuykova, E.:
859   Carbon, nitrogen, and sulfur isotope changes and hydro-geological processes in a saline
860   lake chain. Hydrobiologia, 529, 225-235, 2004.
861   Eckert, T., Brunner, B., Edwards, E. A. and Wortmann, U.G.: Microbially mediated re-oxidation
862   of sulfide during dissimilatory sulfate reduction by *Desulfobacter latus*. Geochim.
863   Cosmochim. Acta, 75(12), 3469-3485, 2011.

864 Farquhar, J., Peters, M., Johnston, D. T., Strauss, H., Masterson, A., Wiechert, U. and Kaufman,
865   A. J.: Isotopic evidence for Mesoarchaean anoxia and changing atmospheric sulphur
866   chemistry. Nature, 449, 706-710, 2007.
867 Fike, D. A. and Grotzinger, J. P.: A paired sulfate-pyrite $\delta^{34}S$ approach to understanding the
868   evolution of the Ediacaran-Cambrian sulfur cycle. Geochim. Cosmochim. Acta, 72, 2636-
869   2648, 2008.
870 Fike, D. A., Grotzinger, J. P., Pratt, L. M. and Summons, R. E.: Oxidation of the Ediacaran Ocean.
871   Nature, 444, 744-747, 2006.
872 Fry, B.: Sources of carbon and sulfur nutrition for consumers in three meromictic lakes of New
873   York State. Limnol. Oceanogr., 31, 79-88, 1986a.
874 Fry, B.: Stable sulfur isotopic distributions and sulfate reduction in lake sediments of the
875   Adirondacks Mountains, New York. Biogeochemistry, 2, 329-343, 1986b.
876 Fry, B., Giblin, A. and Dornblaser, M.: Stable sulfur isotopic compositions of chromium-reducible
877   sulfur in lake sediments, in: Vairavamurthy, A. and Schoonens, M. A. A. (Eds.),
878   Geochemical Transformation of Sedimentary Sulfur, American Chemical Society, ACS
879   Symposium Series, 612, 397-410, 1995.
880 Fry, B., Jannasch, H. W., Molyneaux, S. J., Wirsen, C. O., Muramoto, J. A. and King, S.: Stable
881   isotope studies of the carbon, nitrogen and sulfur cycles in the Black Sea and the Cariaco
882   Trench. Deep-Sea Res., A38(Suppl. 2), S1003-S1019, 1991.
883 Gellatly, A. M. and Lyons, T. W.: Trace sulfate in mid-Proterozoic carbonates and the sulfur
884   isotope record of biospheric evolution. Geochim. Cosmochim. Acta, 69, 3813-3829,
885   2005.
886 Gill, B. C., Lyons, T. W. and Saltzman, M. R.: Parallel, high-resolution carbon and sulfur isotope
887   records of the evolving Paleozoic marine sulfur reservoir. Palaeogeogr. Palaeoclimatol.
888   Palaeoecol., 256, 156-173, 2007.
889 Gill, B. C., Lyons, T. W., Young, S. A., Kump, L. R., Knoll, A. H. and Saltzman, M. R.: Geochemical
890   evidence for widespread euxinia in the Later Cambrian ocean. Nature, 469, 80-83,
891   2011a.
892 Gill, B. C., Lyons, T. W. and Jenkyns, H. C.: A global perturbation to the sulfur cycle during the
893   Toarcian Oceanic Anoxic Event. Earth Planet. Sci. Lett., 312, 484-496, 2011b.
894 Gomes, M. L. and Hurtgen, M. T.: Sulfur isotope systematics of a euxinic, low-sulfate lake:
895   evaluating the importance of the reservoir effect in modern and ancient oceans.
896   Geology, 41, 663-666, 2013.
897 Gorlenko, V. M. and Chebotarev, E. N.: Microbiologic processes in meromictic Lake Sakovo.
898   Microbiology, 50, 134-139, 1981.
899 Gorlenko, V. M., Vainstein, B. and Kachalkin, V. I.: Microbiological characteristic of Lake
900   Mogilnoe. Arch. Hydrobiol., 81, 475-492, 1978.
901 Gradstein, F. M., Ogg, J. G., Schmitz, M. D. and Ogg, G. M.: The Geologic Time Scale 2012.
902   Elsevier, Amsterdam, 2 vol., 2012.
903 Habicht, K. S. and Canfield, D. E.: Sulphur isotope fractionation in modern microbial mats and
904   the evolution of the sulphur cycle. Nature, 382, 342-343, 1996.
905 Habicht, K. S. and Canfield, D. E.: Sulfur isotope fractionation during bacterial sulfate reduction
906   in organic-rich sediments. Geochim. Cosmochim. Acta, 61, 5351-5361, 1997.

907   Habicht, K. S. and Canfield, D. E.: Isotope fractionation by sulfate-reducing natural populations
908   and the isotopic composition of sulfide in marine sediments. Geology, 29, 555-558,
909   2001.
910   Habicht, K. S., Gade, M., Thamdrup, B., Berg, P. and Canfield, D. E.: Calibration of sulfate levels
911   in the Archean ocean. Science, 298, 2372-2374, 2002.
912   Halevy, I., Peters, S. E. and Fischer, W. W.: Sulfate burial constraints on the Phanerozoic sulfur
913   cycle. Science, 337, 331-334, 2012.
914   Halverson, G. P. and Hurtgen, M. T.: Ediacaran growth of the marine sulfate reservoir. Earth
915   Planet. Sci. Lett., 263, 32-44, 2007.
916   Halverson, G. P., Hoffman, P. F., Schrag, D. P., Maloof, A. C. and Rice, A. H. N.: Toward a
917   Neoproterozoic composite carbon-isotope record. Geol. Soc. Am. Bull., 117, 1181-1207,
918   2005.
919   Hartmann, M. and Nielsen, H.: δ^{34}S-Werte in rezenten Meeressedimenten und ihre Deutung am
920   Beispiel einiger Sedimentprofile aus der westlichen Ostsee. Geol. Rundsch., 58, 621-655,
921   1968.
922   Holland, H. D.: Volcanic gases, black smokers, and the Great Oxidation Event. Geochim.
923   Cosmochim. Acta, 66, 3811-3826, 2002.
924   Holser, W., Maynard, J. B. and Cruikshank, K.: Modelling the natural cycle of sulphur through
925   Phanerozoic time, in: Brimblecombe, P. and Lein, A. Y. (Eds.), Evolution of the Global
926   Biogeochemical Sulfur Cycle, Wiley, New York, 21-56, 1989.
927   Horita, J., Zimmermann, H. and Holland, H. D.: Chemical evolution of seawater during the
928   Phanerozoic: Implications from the record of marine evaporites. Geochim. Cosmochim.
929   Acta, 66, 3733-3756, 2002.
930   Hurtgen, M. T., Arthur, M. A., Suits, N. S. and Kaufman, A. J.: The sulfur isotopic composition of
931   Neoproterozoic seawater sulfate: implications for a snowball Earth? Earth Planet. Sci.
932   Lett., 203, 413-429, 2002.
933   Hurtgen, M. T., Arthur, M. A. and Halverson, G. P.: Neoproterozoic sulfur isotopes, the
934   evolution of microbial sulfur species, and the burial efficiency of sulfide as sedimentary
935   pyrite. Geology, 33, 41-44, 2005.
936   Hurtgen, M. T., Halverson, G. P., Arthur, M. A. and Hoffman, P. F.: Sulfur cycling in the
937   aftermath of a 635-Ma snowball glaciation: Evidence for a syn-glacial sulfidic deep
938   ocean. Earth Planet. Sci. Lett., 245, 551-570, 2006.
939   Ivanov, M. V., Rusanov, I. I., Pimenov, N. V., Bairamov, I. T., Yusupov, S. K., Savvichev, A. S., Lein,
940   A. Y. and Sapozhnikov, V. V.: Microbial processes of the carbon and sulfur cycles in Lake
941   Mogil'noe. Microbiology, 70, 583-593, 2001.
942   Johnston, D. T.: Multiple sulfur isotopes and the evolution of Earth's surface sulfur cycle. Earth-
943   Sci. Rev., 106, 161-183, 2011.
944   Johnston, D. T., Wing, B. A., Farquhar, J., Kaufman, A. J., Strauss, H., Lyons, T. W., Kah, L. C. and
945   Canfield, D. E.: Active microbial sulfur disproportionation in the Mesoproterozoic.
946   Science, 310, 1477-1479, 2005.
947   Johnston, D. T., Farquhar, J., Habicht, K. S. and Canfield, D. E.: Sulphur isotopes and the search
948   for life: strategies for identifying sulphur metabolisms in the rock record and beyond.
949   Geobiology, 6, 425-435, 2008.

950 Jones, B. A., Facchetti, A., Wasielewski, M. R. and Marks, T. J.: Theory of oxidation-reduction
951   reactions involving electron transfer. 5. Comparison and properties of electrochemical
952   and chemical rate constants. J. Am. Chem. Soc., 129, 15259-15278, 2007.
953 Jørgensen, B. B.: Mineralization of organic matter in the sea bed—the role of sulphate
954   reduction. Nature, 296, 643-645, 1982.
955 Jørgensen, B. B. and Cohen, Y.: Solar Lake (Sinai). 5. The sulfur cycle of the benthic
956   cyanobacterial mats. Limnol. Oceanogr., 22, 657-666, 1977.
957 Kah, L. C., Lyons, T. W. and Frank, T. D.: Low marine sulphate and protracted oxygenation of the
958   Proterozoic biosphere. Nature, 431, 834-838, 2004.
959 Kampschulte, A. and Strauss, H.: The sulfur isotopic evolution of Phanerozoic seawater based
960   on the analysis of structurally substituted sulfate in carbonates. Chem. Geol., 204, 255-
961   286, 2004.
962 Kamyshny, A., Jr., Zerkle, A. L., Mansaray, Z. F., Ciglenečki, I., Bura-Nakić, E., Farquhar, J. and
963   Ferdelman, T. G.: Biogeochemical sulfur cycling in the water column of a shallow
964   stratified sea-water lake: speciation and quadruple sulfur isotope composition. Mar.
965   Geol., 127, 144-154, 2011.
966 Kaplan, I. R.: Stable isotopes of sulfur, nitrogen and deuterium in Recent marine environments,
967   in: Arthur, M. A., et al. (Eds.), Stable Isotopes in Sedimentary Geology, Society for
968   Sedimentary Geology, Tulsa, Oklahoma, 21-108, 1983.
969 Kapan, I. R. and Rittenberg, S. C.: Microbiological fractionation of sulphur isotopes. J. Gen.
970   Microbiol., 34, 195-212, 1964.
971 Kaplan, I. R., Emery, K. O. and Rittenberg, S. C.: The distribution and isotopic abundance of
972   sulphur in recent marine sediments off southern California. Geochim. Cosmochim. Acta,
973   27, 297-331, 1963.
974 Karcz, P.: Relationships between development of organic-rich shallow shelf facies and variation
975   in isotopic composition of pyrite (Middle Triassic, Spitsbergen). Polish Polar Research,
976   31, 239-254, 2010.
977 Karube, Z., Okada, N. and Tayasu, I.: Sulfur stable isotope signature identifies the source of
978   reduced sulfur in benthic communities in macrophyte zones of Lake Biwa, Japan.
979   Limnology, 13, 269-280, 2012.
980 Kemp, A. L. W. and Thode, H. G.: The mechanism of the bacterial reduction of sulphate and
981   sulphite from isotope fractionation studies. Geochim. Cosmochim. Acta, 32, 71-91,
982   1968.
983 Kleikemper, J., Schroth, M. H., Bernasconi, S. M., Brunner, B. and Zeyer, J.: Sulfur isotope
984   fractionation during growth of sulfate-reducing bacteria on various carbon sources.
985   Geochim. Cosmochim. Acta, 68, 4891-4904, 2004.
986 Ku, T. C. W., Walter, L. M., Coleman, M. L., Blake, R. E. and Martini, A. M.: Coupling between
987   sulfur recycling and syndepositional carbonate dissolution: evidence from oxygen and
988   sulfur isotope composition of pore water sulfate, South Florida Platform, U.S.A.
989   Geochim. Cosmochim. Acta, 63, 2529-2546, 1999.
990 Kump, L. R. and Arthur, M. A.: Interpreting carbon-isotope excursions: carbonates and organic
991   matter. Chem. Geol., 161, 181-198, 1999.
992 Kurtz, A. C., Kump, L. R., Arthur, M. A., Zachos, J. C. and Paytan, A.: Early Cenozoic decoupling of
993   the global carbon and sulfur cycles. Paleoceanography, 18, PA000908, 2003.

994 Leavitt, W. D., Halevy, I., Bradley, A. S. and Johnston, D. T.: Influence of sulfate reduction rates
995   on the Phanerozoic sulfur isotope record. Proc. Nat. Acad. Sci. (U.S.A.) , 110(28), 11244-
996   11249, 2013.
997 Lee, Y. J. and Lwiza, K.: Interannual variability of temperature and salinity in shallow water: Long
998   Island Sound, New York. J. Geophys. Res., 110, C09022, 2005.
999 Lein, A. Y.: Biogeochemistry of the anaerobic diagenesis of Recent Baltic Sea sediments.
1000   Environ. Biogeochem., 35, 441-461, 1983.
1001 Li, C., Love, G. D., Lyons, T. W., Fike, D. A., Sessions, A. L. and Chu, X.: A stratified redox model
1002   for the Ediacaran ocean. Science, 328, 80-83, 2010.
1003 Li, X., Gilhooly, W. P., III, Zerkle, A. L., Lyons, T. W., Farquhar, J., Werne, J. P., Varela, R. and
1004   Scranton, M. I.: Stable sulfur isotopes in the water column of the Cariaco Basin.
1005   Geochim. Cosmochim. Acta, 74, 6764-6778, 2010.
1006 Llobet-Brossa, E., Rabus, R., Böttcher, M. E., Könneke, M., Finke, N., Schramm, A., Meyer, R. L.,
1007   Grötzschel, S., Rosselló-Mora, R. and Amann, R.: Community structure and activity of
1008   sulfate-reducing bacteria in an intertidal surface sediment: a multi-method approach.
1009   Aquat. Microbial Ecol., 29, 211-226, 2002.
1010 Lojen, S., Ogrinc, N., Dolenec, T., Vokal, B., Szaran, J., Mihelčić, G. and Branica, M.: Nutrient
1011   fluxes and sulfur cycling in the organic-rich sediment of Makirina Bay (Central Dalmatia,
1012   Croatia). Sci. Total Environ., 327, 265-284, 2004.
1013 Lowenstein, T. K., Hardie, L. A., Timofeeff, M. N. and Demicco, R. V.: Secular variation in
1014   seawater chemistry and the origin of calcium chloride basinal brines. Geology, 31, 857-
1015   860, 2003.
1016 Lowenstein, T. K., Timofeeff, M. N., Kovalevych, V. M. and Horita, J.: The major-ion composition
1017   of Permian seawater. Geochim. Cosmochim. Acta, 69, 1701-1719, 2005.
1018 Loyd, S. J., Marenco, P. J., Hagadorn, J. W., Lyons, T. W., Kaufman, A. J., Sour-Tovar, F. and
1019   Corsetti, F. A.: Sustained low marine sulfate concentrations from the Neoproterozoic to
1020   the Cambrian: insights from carbonates of northwestern Mexico and eastern California.
1021   Earth Planet. Sci. Lett., 339-340, 79-94, 2012.
1022 Loyd, S. J., Marenco, P. J., Hagadorn, J. W., Lyons, T. W., Kaufman, A. J., Sour-Tovar, F. and
1023   Corsetti, F. A.: Local δ^{34}S variability in ~580 Ma carbonates of northwestern Mexico and
1024   the Neoproterozoic marine sulfate reservoir. Precambr. Res., 224, 551-569, 2013.
1025 Luo, G. M., Kump, L. R., Wang, Y., Tong, J., Arthur, M. A., Yang, H., Huang, J., Yin, H. and Xie, S.:
1026   Isotopic evidence for an anomalously low oceanic sulphate concentration following end-
1027   Permian mass extinction. Earth Planet. Sci. Lett., 300, 101-111, 2010.
1028 Luo, G. M., Ono, S., Algeo, T. J., Huang, J., Li, C., Zhou, L., Liu, J. and Xie, S.C.: Return of Archean
1029   low oceanic sulfate levels during the earliest Mesoproterozoic. Precambr. Res., 258, 36-
1030   47, 2015.
1031 Lyons, T. W.: Sulfur isotopic trends and pathways of iron sulfide formation in upper Holocene
1032   sediments of the anoxic Black Sea. Geochim. Cosmochim. Acta, 61, 3367-3382, 1997.
1033 Lyons, T. W. and Gill, B. C.: Ancient sulfur cycling and oxygenation of the early biosphere.
1034   Elements 6, 93-99, 2010.
1035 Lyons, T. W. and Severmann, S.: A critical look at iron paleoredox proxies: New insights from
1036   modern euxinic marine basins. Geochim. Cosmochim. Acta, 70, 5698-5722, 2006.

1037 Mandernack, K. W., Krouse, H. R. and Skei, J. M.: A stable sulfur and oxygen isotopic
1038   investigation of sulfur cycling in an anoxic marine basin, Framvaren Fjord, Norway.
1039   Chem. Geol., 195, 181-200, 2003.
1040 Mandernack, K. W., Lynch, L., Krouse, H. R. and Morgan, M. D.: Sulfur cycling in wetland peat of
1041   the New Jersey Pinelands and its effect on stream water chemistry. Geochim.
1042   Cosmochim. Acta, 64, 3949-3964, 2000.
1043 Matrosov, A. G., Chebotarev, N. Ye, Kudryavtseva, A. J., Zyakun, A. M. and Ivanov, M. V.: Sulfur
1044   isotopic composition in freshwater lakes containing H_2S. Geokhimiya, 6, 943-7, 1975,
1045   and Geochem. Internat., 12, 217-21, 1975.
1046 Mayer, B. and Schwark, L.: A 15,000-year stable isotope record from sediments of Lake
1047   Steisslingen, southwest Germany. Chem. Geol., 161, 315-337, 1999.
1048 McArthur, J. M., Donovan, D. T., Thirlwall, M. F., Fouke, B. W. and Mattey, D.: Strontium isotope
1049   profile of the early Toarcian (Jurassic) oceanic anoxic event, the duration of ammonite
1050   biozones, and belmenite palaeotemperatures. Earth Planet. Sci. Lett., 179, 269-285,
1051   2000.
1052 McFadden, K. A., Huang, J., Chu, X., Jiang, G., Kaufman, A. J., Zhou, C., Yuan, X. and Xiao, S.:
1053   Pulsed oxidation and biological evolution in the Ediacaran Doushantuo Formation. Proc.
1054   Nat. Acad. Sci. (U.S.A.), 105, 3197-3202, 2008.
1055 Millero, F. J.: Chemical Oceanography, 3rd ed., CRC Press, Boca Raton, Florida, 2005.
1056 Montañez, I.P., et al.: Understanding Earth's Deep Past: Lessons for Our Climate Future,
1057   National Academy of Sciences Press, Washington, D.C., 2011.
1058 Nakagawa, M., Ueno, Y., Hattori, S., Umemura, M., Yagi, A., Takai, K., Koba, K., Sasaki, Y.,
1059   Makabe, A. and Yoshida, N.: Seasonal change in microbial sulfur cycling in monomictic
1060   Lake Fukami-ike, Japan. Limnol. Oceanogr., 57, 974-988, 2012.
1061 Nakai, N. and Jensen, M. L.: The kinetic isotope effect in the bacterial reduction and oxidation
1062   of sulfur. Geochim. Cosmochim. Acta, 28, 1893-1912, 1964.
1063 Nakai, N., Wada, H., Kiyosu, Y. and Takimoto, M.: Stable isotope studies on the origin and
1064   geological history of water and salts in the Lake Vanda area, Antarctica. Geochem. Jour.,
1065   9, 7-24, 1975.
1066 Nakano, T., Tayasu, I., Yamada, Y., Hosono, T., Igeta, A., Hyodo, F., Ando, A., Saitoh, Y., Tanaka,
1067   T., Wada, E. and Yachi, S.: Effect of agriculture on water quality of Lake Biwa tributaries,
1068   Japan. Sci. Total Environ., 389, 132-148, 2008.
1069 Newton, R. J., Reeves, E. P., Kafousia, N., Wignall, P. B., Bottrell, S. H. and Sha, J.-G.: Low marine
1070   sulfate concentrations and the isolation of the European epicontinental sea during the
1071   Early Jurassic. Geology, 39, 7-10, 2011.
1072 Nriagu, J. O. and Coker, R. D.: Emission of sulfur from Lake Ontario sediments. Limnol.
1073   Oceanogr., 21, 485-489, 1976.
1074 Nriagu, J. O. and Harvey, H. H.: Isotopic variation as an index of sulfur poiiution in lakes around
1075   Sudbury, Ontario. Nature, 273, 223-224, 1978.
1076 Nriagu, J. O. and Soon, Y. K.: Distribution and isotopic composition of sulfur in lake sediments of
1077   northern Ontario. Geochim. Cosmochim. Acta, 49, 823-834, 1985.
1078 Oren, A.: Bioenergetic aspects of halophilism. Microbiol. Mol. Biol. Rev., 63, 334-348, 1999.
1079 Overmann, J., Beatty, J. T., Krouse, H. R. and Hall, K. J.: The sulfur cycle in the chemocline of a
1080   meromictic salt lake. Limnol. Oceanogr., 41, 147-156, 1996.

1081 Owens, J. D., Gill, B. C., Jenkyns, H. C., Bates, S. M., Severmann, S., Kuypers, M. M. M.,
1082   Woodfine, R. G. and Lyons, T. W.: Sulfur isotopes track the global extent and dynamics
1083   of euxinia during Cretaceous Oceanic Anoxic Event 2. Proc. Nat. Acad. Sci. (U.S.A.), 110,
1084   18407-18412, 2013.
1085 Paytan, A., Kastner, M., Campbell, D. and Thiemens, M. H.: Sulfur isotopic composition of
1086   Cenozoic seawater sulfate. Science, 282, 1459-1462, 1998.
1087 Paytan, A., Kastner, M., Campbell, D. and Thiemens, M. H.: Seawater sulfur isotope fluctuations
1088   in the Cretaceous. Science, 304, 1663-1665, 2004.
1089 Peterson, B. J. and Howarth, R. W.: Sulfur, carbon, and nitrogen isotopes used to trace organic
1090   matter flow in the salt-march estuaries of Sapelo Island, Georgia. Limnol. Oceanogr., 32,
1091   1195-1213, 1987.
1092 Planavsky, N. J., Bekker, A., Hofmann, A., Owens, J. D. and Lyons, T. W.: Sulfur record of rising
1093   and falling marine oxygen and sulfate levels during the Lomagundi event. Proc. Nat.
1094   Acad. Sci. (U.S.A.), 109, 18300-18305, 2012.
1095 Price, F. T. and Casagrande, D. J.: Sulfur distribution and isotopic composition in peats from the
1096   Okefenokee Swamp, Georgia and the Everglades, Florida. Internat. J. Coal Geol., 17, 1-
1097   20, 1991.
1098 Purdy, K., Hawes, I., Bryant, C. L., Fallick, A. E. and Nedwell, D. B.: Estimates of sulphate
1099   reduction rates in Lake Vanda, Antarctica support the proposed recent history of the
1100   lake. Antarct. Sci., 13, 393, 2001.
1101 Rees, C.E.: A steady-state model for sulphur isotope fractionation in bacterial reduction
1102   processes. Geochim. Cosmochim. Acta 27, 1141-1162, 1973.
1103 Rickard, D. T.: Kinetics and mechanism of pyrite formation at low temperatures. Am. J. Sci.,
1104   275(6), 636-652, 1975.
1105 Ries, J. B., Fike, D. A., Pratt, L. M., Lyons, T. W. and Grotzinger, J. P.: Superheavy pyrite
1106   ($\delta^{34}S_{pyr}>\delta^{34}S_{CAS}$) in the terminal Proterozoic Nama Group, southern Namibia: a
1107   consequence of low seawater sulfate at the dawn of life. Geology, 37, 743-746, 2009.
1108 Röhl, H.-J., Schmid-Röhl, A., Oschmann, W., Frimmel, A. and Schwark, L.: The Posidonia Shale
1109   (Lower Toarcian) of SW-Germany: an oxygen-depleted ecosystem controlled by sea level
1110   and palaeoclimate. Palaeogeogr. Palaeoclimatol. Palaeoecol. 165, 27-52, 2001.
1111 Rudnicki, M. D., Elderfield, H. and Spiro, B.: Fractionation of sulfur isotopes during bacterial
1112   sulfate reduction in deep ocean sediments at elevated temperatures. Geochim.
1113   Cosmochim. Acta, 65(5), 777–789, 2001.
1114 Scheiderich, K., Zerkle, A. L., Helz, G. R., Farquhar, J. and Walker, R. J.: Molybdenum isotope,
1115   multiple sulfur isotope, and redox-sensitive element behavior in early Pleistocene
1116   Mediterranean sapropels. Chem. Geol., 279, 134-144, 2010.
1117 Shen, Y. A., Buick, R. and Canfield, D. E.: Isotopic evidence for microbial sulphate reduction in
1118   the early Archaean era. Nature, 410, 77-81, 2001.
1119 Sim, M. S., Bosak, T. and Ono, S. H.: Large sulfur isotope fractionation does not require
1120   disproportionation. Science, 333, 74-78, 2011a.
1121 Sim, M. S., Ono, S. H., Donovan, K., Templer, S. P. and Bosak, T.: Effect of electron donors on the
1122   fractionation of sulfur isotopes by a marine *Desulfovibrio* sp. Geochim. Cosmochim.
1123   Acta, 75, 4244-4259, 2011b.

1124 Song, H. Y., Tong, J., Algeo, T. J., Song, H. J., Qiu, H., Zhu, Y., Tian, L., Bates, S., Lyons, T. W., Luo,
1125   G. M. and Kump, L. R.: Early Triassic seawater sulfate drawdown. Geochim. Cosmochim.
1126   Acta, 128, 95-113, 2014.
1127 Sørensen, K. B. and Canfield, D. E.: Annual fluctuations in sulfur isotope fractionation in the
1128   water column of a euxinic marine basin. Geochim. Cosmochim. Acta, 68, 503-515, 2004.
1129 Stam, M. C., Mason, P. R. D., Pallud, C. and Van Cappellen, P.: Sulfate reducing activity and
1130   sulfur isotope fractionation by natural microbial communities in sediments of a
1131   hypersaline soda lake (Mono Lake, California). Chem. Geol., 278, 23-30, 2010.
1132 Sternbeck, J. and Sohlenius, G.: Authigenic sulfide and carbonate mineral formation in Holocene
1133   sediments of the Baltic Sea. Chem. Geol., 135, 55-73, 1997.
1134 Strauss, H.: The isotopic composition of sedimentary sulfur through time. Palaeogeogr.
1135   Palaeoclimatol. Palaeoecol. 132, 97-118, 1997.
1136 Strauss, H.: Geological evolution from isotope proxy signals—sulfur. Chem. Geol., 161, 89-101,
1137   1999.
1138 Strauss, H.: Sulfur isotopes and the early Archaean sulphur cycle. Precambr. Res., 126, 349-361,
1139   2003.
1140 Stribling, J. M., Cornwell, J. C. and Currin, C.: Variability of stable sulfur isotopic ratios in
1141   *Spartina alterniflora*. Mar. Ecol. Progr. Ser., 166, 73-81, 1998.
1142 Suits, N. S. and Wilkin, R. T.: Pyrite formation in the water column and sediments of a
1143   meromictic lake. Geology, 26, 1099-1102, 1998.
1144 Sweeney, R. E. and Kaplan, I. R.: Stable isotope composition of dissolved sulfate and hydrogen
1145   sulfide in the Black Sea. Mar. Chem., 9, 145-152, 1980.
1146 Valentine, D. L.: Biogeochemistry and microbial ecology of methane oxidation in anoxic
1147   environments: a review. Antonie van Leeuwenhoek, 81, 271-282, 2002.
1148 Wacey, D., McLoughlin, N., Whitehouse, M. J. and Kilburn, M. R.: Two coexisting sulfur
1149   metabolisms in a ca. 3400 Ma sandstone. Geology, 38, 1115-1118, 2010.
1150 Werne, J. P., Hollander, D. J., Behrens, A., Schaeffer, P., Albrecht, P. and Damsté, J. S. S.: Timing
1151   of early diagenetic sulfurization of organic matter: A precursor-product relationship in
1152   Holocene sediments of the anoxic Cariaco Basin, Venezuela. Geochim. Cosmochim. Acta,
1153   64, 1741-1751, 2000.
1154 Werne, J. P., Lyons, T. W., Hollander, D. J., Formolo, M. J. and Damsté, J. S. S.: Reduced sulfur in
1155   euxinic sediments of the Cariaco Basin: sulfur isotope constraints on organic sulfur
1156   formation. Chem. Geol., 195, 159-179, 2003.
1157 Werne, J. P., Lyons, T. W., Hollander, D. J., Schouten, S., Hopmans, E. C. and Damsté, J. S. S.:
1158   Investigating pathways of diagenetic organic matter sulfurization using compound-
1159   specific sulfur isotope analysis. Geochim. Cosmochim. Acta, 72, 3489-3502, 2008.
1160 Wijsman, J. W. M., Middelburg, J. J., Herman, P. M. J., Böttcher, M. E. and Heip, C. H. R.: Sulfur
1161   and iron speciation in surface sediments along the northwestern margin of the Black
1162   Sea. Mar. Chem., 74, 261-278, 2001.
1163 Wilkin, R. T., Barnes, H .L. and Brantley, S.L.: The size distribution of framboidal pyrite in marine
1164   sediments: an indicator of redox conditions. Geochim. Cosmochim. Acta, 60, 3897-3912,
1165   1996.
1166 Wortmann, U. G. and Chernyavsky, B. M.: Effect of evaporite deposition on Early Cretaceous
1167   carbon and sulphur cycling. Nature, 446, 654-656, 2007.

1168   Wortmann, U. G. and Paytan, A.: Rapid variability of seawater chemistry over the past 130
1169   million years. Science, 337, 334-336, 2012.

1170   Wortmann, U. G., Bernasconi, S. M. and Böttcher, M. E.: Hypersulfidic deep biosphere indicates
1171   extreme sulfur isotope fractionation during single-step microbial sulfate reduction.
1172   Geology, 29, 647-650, 2001.

1173   Wotte, T., Strauss, H., Fugmann, A. and Garbe-Schönberg, D.: Paired $\delta^{34}S$ data from carbonate-
1174   associated sulfate and chromium-reducible sulfur across the traditional Lower-Middle
1175   Cambrian boundary of W-Gondwana. Geochim. Cosmochim. Acta, 85, 228-253, 2012.

1176   Wu, N., Farquhar, J., Strauss, H., Kim, S.-T. and Canfield, D. E.: Evaluating the S-isotope
1177   fractionation associated with Phanerozoic pyrite burial. Geochim. Cosmochim. Acta, 74,
1178   2053-2071, 2010.

1179   Zaback, D. A. and Pratt, L. M.: Isotopic composition and speciation of sulfur in the Miocene
1180   Monterey Formation: Reevaluation of sulfur reactions during early diagenesis in marine
1181   environments. Geochim. Cosmochim. Acta, 56, 763-774, 1992.

1182   Zerkle, A. L., Kamyshny, A., Jr., Kump, L. R., Farquhar, J., Oduro, H. and Arthur, M. A.: Sulfur
1183   cycling in a stratified euxinic lake with moderately high sulfate: Constraints from
1184   quadrupole S isotopes. Geochim. Cosmochim. Acta, 74, 4953-4970, 2010.

1185   Zhang, S., Jiang, G., Zhang, J., Song, B., Kennedy, M. J. and Christie-Blick, N.: U-Pb sensitive high-
1186   resolution ion microprobe ages from the Doushantuo Formation in south China:
1187   constraints on late Neoproterozoic glaciations. Geology, 33, 473-476, 2005.

1188   Zhang, S., Jiang, G. and Han, Y.: The age of the Nantuo Formation and Nantuo glaciation in
1189   South China. Terra Nova, 20, 289-294, 2008.

1190

Figure captions

Fig. 1. The rate method. On a crossplot of aqueous sulfate concentration ($[SO_4^{2-}]_{aq}$) versus S-isotopic fractionation between cogenetic sulfate and sulfide ($\Delta^{34}S_{sulfate-sulfide}$), the diagonal blue lines represent maximum rates of change in sulfate $\delta^{34}S$ (i.e., $\partial\delta^{34}S_{SO4}/\partial t(max)$). For paleomarine systems, maximum seawater sulfate concentrations ($[SO_4^{2-}]_{SW}(max)$) can be estimated from the abscissa based on measured values of $\Delta^{34}S_{CAS-PY}$ and $\partial\delta^{34}S_{CAS}/\partial t(max)$. The two scales on the abscissa represent $[SO_4^{2-}]_{SW}$ in oxic (O) and anoxic (A) oceans, in which pyrite burial fluxes are equal to 4×10^{13} g yr^{-1} and 10×10^{13} g yr^{-1} (i.e., 40% and 100% of the modern total sulfur sink flux), respectively. The typical range of $\Delta^{34}S_{sulfate-sulfide}$ due to MSR fractionation in modern marine systems is 30-60‰ (Habicht and Canfield, 1997). The maximum rate of seawater sulfate $\delta^{34}S$ variation during the Cenozoic is ~0.7‰ Myr^{-1} (Paytan et al., 1998), yielding estimates of ~40-80 mM for $[SO_4^{2-}]_{SW}$ through projection to the abscissa (dashed lines). These estimates exceed actual modern seawater $[SO_4^{2-}]$, which is ~29 mM (Millero, 2005) because the *measured* maximum rate of $\partial\delta^{34}S_{SO4}/\partial t$ (light blue parallelogram) is less than the *theoretical* possible maximum rate (~1-2‰ Myr^{-1}; red parallelogram).

Fig. 2. The MSR-trend method. **(a)** Data from 81 modern aqueous systems (Table A1). The non-hypersaline environments (n = 75) yield a linear regression (solid line; y = 0.42x + 1.10 in log units) having r = +0.90 (t-statistic = 1.99, ($p(\alpha)$ <0.01) and a limited uncertainty range (dashed lines). The MSR trend thus represents a process with an order of reaction (n) of 0.42 and a rate constant (k) of 1.10 (cf. Jones et al., 2007). The gray field encloses most of the data from Table A1 and highlights the overall trend. Analysis of the dataset by redox environment yielded statistically indistinguishable trends for oxic (y = 0.48x + 1.10; r = +0.88, n = 44, $p(\alpha)$ <0.01) and euxinic settings (y = 0.40x + 1.06; r = +0.89, n = 31, $p(\alpha)$ <0.01). The Habicht et al. (2002) dataset of 60 sulfate-reducing microbial (SRM) culture values is shown for comparison; these data have been converted to log-log format, and data points that are off scale (i.e., $\Delta^{34}S_{sulfate-sulfide}$ <1‰) are shown by triangles on the abscissa. Neither the six hypersaline environments in our dataset (red symbols) nor the Habicht et al. data (small open circles) were included in the regression analysis. **(b)** Use of the MSR trend to estimate paleo-seawater $[SO_4^{2-}]_{aq}$. Measured values of $\Delta^{34}S_{sulfate-sulfide}$ are projected from the ordinal scale to the MSR trend and then to the abscissa. Note that uncertainty in the slope of the MSR trend is accommodated by projection to the upper uncertainty limit for $\Delta^{34}S_{sulfate-sulfide}$ maxima and to the lower uncertainty limit for $\Delta^{34}S_{sulfate-sulfide}$ minima. The vertical black bar at $[SO_4^{2-}]_{aq}$ = 1.45 (i.e., the modern seawater sulfate concentration of 29 mM) represents the range of F_{MSR} variation among modern marine SRM communities.

Fig. 3. (a) Phanerozoic seawater sulfate $\delta^{34}S$. Data sources: Cenozoic (Paytan et al., 1998; red circles), Cretaceous (Paytan et al., 2004; black squares), and pre-Cretaceous (Kampschulte and Strauss, 2004; blue triangles; Table A2). Secular variation in $\delta^{34}S_{SO4-SW}$ is shown by a mean LOWESS curve (blue line for low-resolution (5-Myr) and red line for high-resolution (1-Myr) records) and a standard deviation ($\pm1\sigma$) range (green field for low-resolution record;

1234   Table A3). Pre-Cretaceous and Cretaceous-Cenozoic estimates of $\delta^{34}S_{SO4-SW}$ have
1235   uncertainties of ±2-7‰ and ±<1‰, respectively. The labels represent four short-term (<2-
1236   Myr) intervals of high-frequency $\partial\delta^{34}S_{SO4}/\partial t$ variation (EMCB = Early-Middle Cambrian
1237   boundary; SPICE = Steptoean positive carbon isotope excursion; CTB = Cenomanian-Turonian
1238   boundary). **(b)** Rate of seawater $\delta^{34}S$ variation ($\partial\delta^{34}S_{SO4}/\partial t$) as calculated from the seawater
1239   sulfate $\delta^{34}S$ LOWESS curves. The maximum Phanerozoic $\partial\delta^{34}S_{SO4}/\partial t$ is <4‰ Myr^{-1}, although
1240   rates of 10 to >50‰ Myr^{-1} have been reported from some high-resolution CAS studies. **(c)**
1241 $\Delta^{34}S_{CAS-PY}$ for Phanerozoic marine sediments (data from figure 3 of Wu et al., 2010). The
1242   continental glaciation record is adapted from Montañez et al. (2011); all ages were
1243   converted to the Gradstein et al. (2012) timescale.

1244

1245   **Fig. 4.** Phanerozoic seawater [SO_4^{2-}] (Table A3). The MSR-trend method (Eqs. 6-8) yields an
1246   estimate of mean [SO_4^{2-}]$_{SW}$ (blue curve; bracketed by a ±1σ band). The rate method (Eqs. 3-
1247   4) yields the maximum possible [SO_4^{2-}]$_{SW}$; the black and red curves show maximum values
1248   based on the low- and high-frequency Phanerozoic $\delta^{34}S_{CAS}$ records, respectively (Fig. 3a), and
1249   the dashed red line represents the lower envelope of the high-frequency curve. The modern
1250   seawater [SO_4^{2-}] of ~29 mM is shown by the red arrow.

1251

1252   **Fig. 5.** Comparison of Phanerozoic seawater sulfate [SO_4^{2-}] records. The mean trend of the
1253   present study is shown by a heavy blue line, with the ±1σ uncertainty range shown as a blue
1254   band. Estimates are based either on fluid-inclusion studies (Horita et al., 2002; Brennan et
1255   al., 2004; Lowenstein et al., 2005) or C-S-cycle modeling (Holser et al., 1989; Berner, 2004;
1256   Gill et al., 2007; Wortmann and Chernyavsky, 2007; Wortmann and Paytan, 2012; Halevy et
1257   al., 2012). Arrows indicate unconstrained minimum or maximum values.

1258

1259   **Fig. 6.** Analysis of seawater sulfate concentrations for 10 late Neoproterozoic marine units.
1260   The parallelogram for each unit was generated using the rate method. A summary of results
1261   and data sources is given in Table A4; other details as in Figures 1-2.

1262

1263   **Fig. 7.** Analysis of seawater sulfate concentrations for 8 Paleozoic marine units. The
1264   parallelogram for each unit was generated using the rate method. The red field represents
1265   the long-term average $\Delta^{34}S_{CAS-PY}$ for the Paleozoic based on data in Wu et al. (2010). A
1266   summary of results and data sources is given in Table A4; other details as in Figures 1-2.

1267

1268   **Fig. 8.** Analysis of seawater sulfate concentrations for 8 Mesozoic-Cenozoic marine units. The
1269   parallelogram for each unit was generated using the rate method. The red field represents
1270   the long-term average $\Delta^{34}S_{CAS-PY}$ for the Mesozoic-Cenozoic based on data in Wu et al.
1271   (2010). A summary of results and data sources is given in Table A4; other details as in
1272   Figures 1-2.

1273

1274   **Fig. 9.** Interpretation of deviations in [SO_4^{2-}]$_{SW}$ estimates between the rate and MSR-trend
1275   methods. Type I deviations, in which rate-method estimates are anomalously high (lower
1276   right field), are likely to reflect extremely stable environmental conditions, in which the

1277   marine sulfur cycle is in equilibrium (i.e., balanced source and sink fluxes). Type II

1278   deviations, in which rate-based estimates are anomalously low (upper left field), are likely to

1279   reflect sulfate reduction in semi-restricted marine basins. In this case, $\Delta^{34}S_{CAS-PY}$ will be

1280   controlled by $[SO_4^{2-}]_{SW}$, which may be equal or close to that of the global ocean, but

1281 $\partial\delta^{34}S_{CAS}/\partial t(max)$ will be controlled by the mass of aqueous sulfate within the restricted

1282   basin, which will be a function of basin volume.

1283

1284   **Fig. 10.** Seawater sulfate concentrations for late Neoproterozoic and Phanerozoic marine units

1285   (Figs. 6-8) compared with long-term $[SO_4^{2-}]_{SW}$ curve (Fig. 4). Estimates of $[SO_4^{2-}]_{SW}$ are

1286   based on (1) the rate method (calculated per Eqs. 3-4; shown as open boxes) and (2) the

1287   MSR-trend method (calculated per Eqs. 6-8; shown as solid boxes); note that unit symbols

1288   and colors are keyed to Table A4 and Figures 6-8. See text for discussion. Other details as in
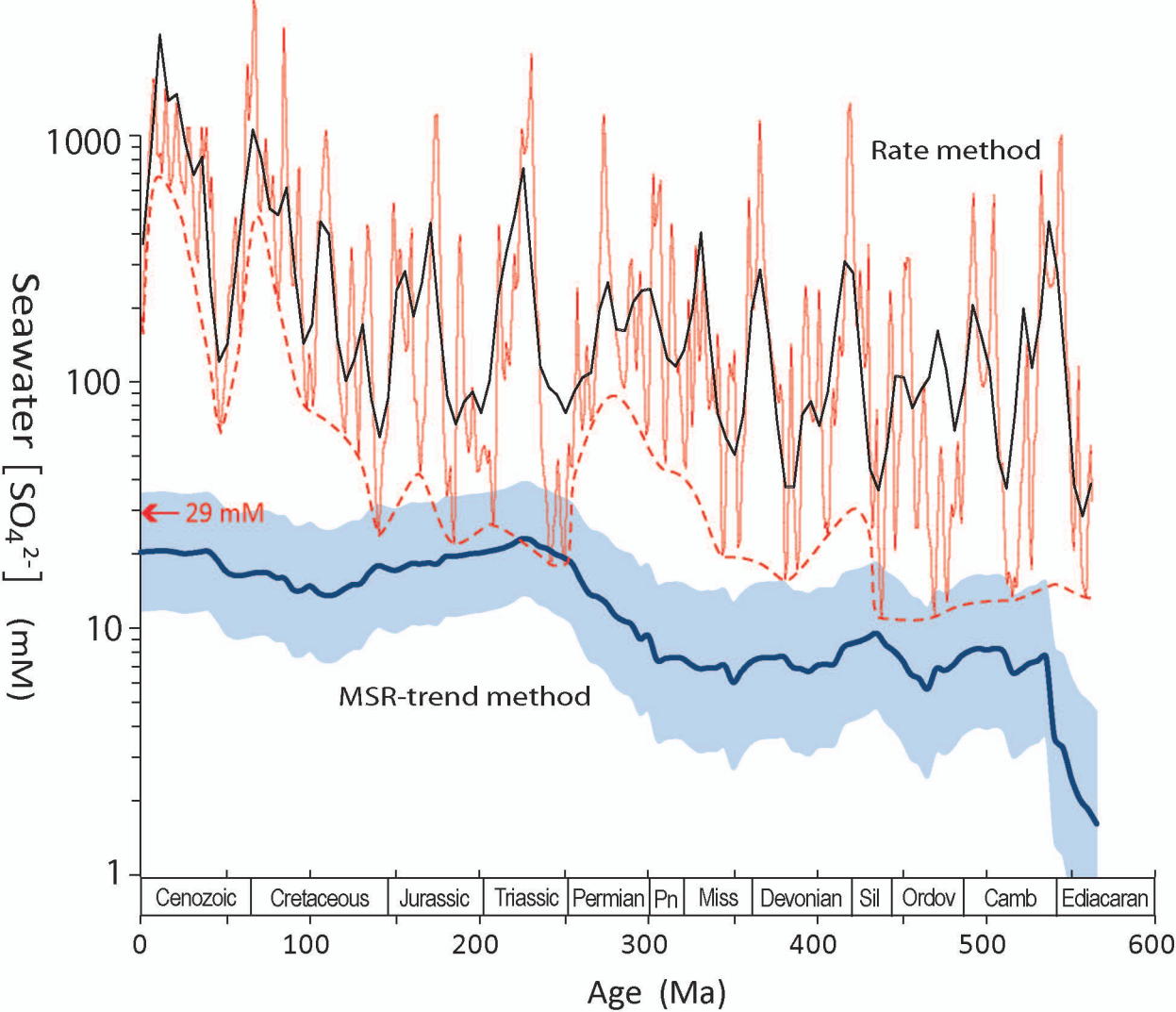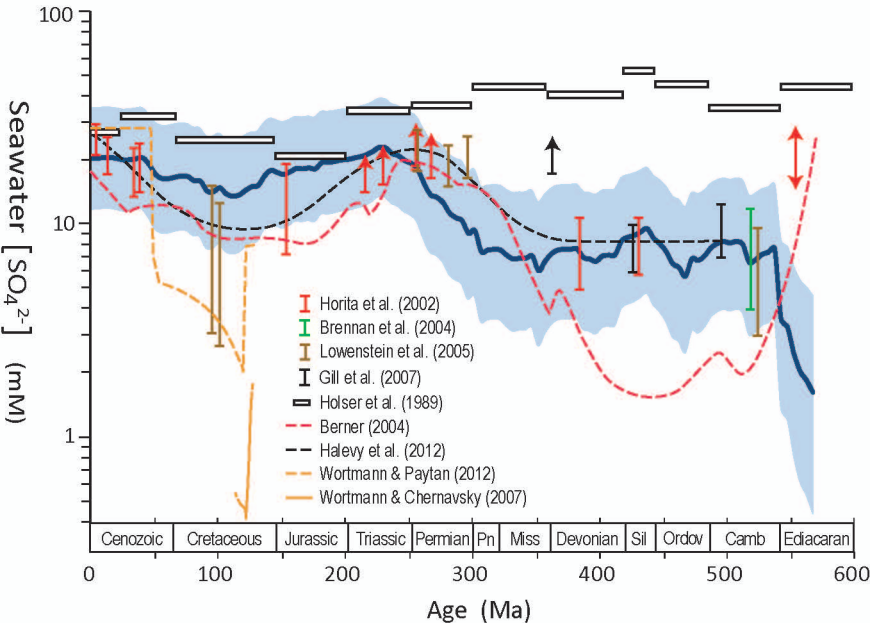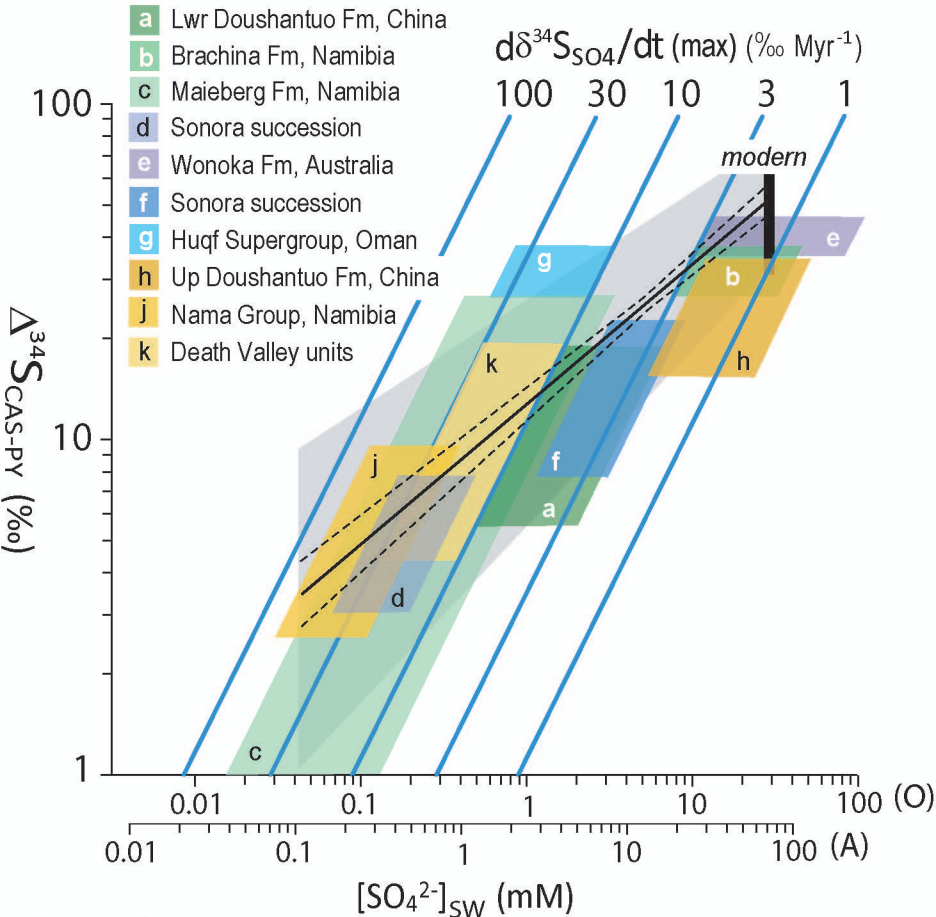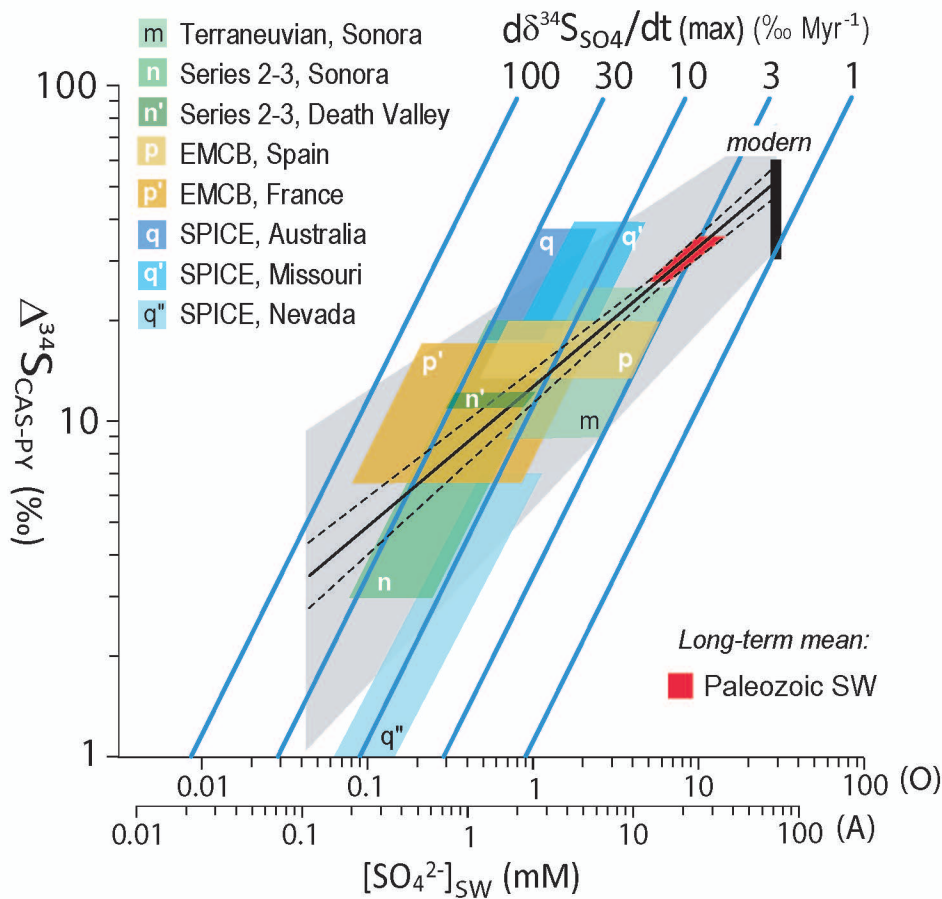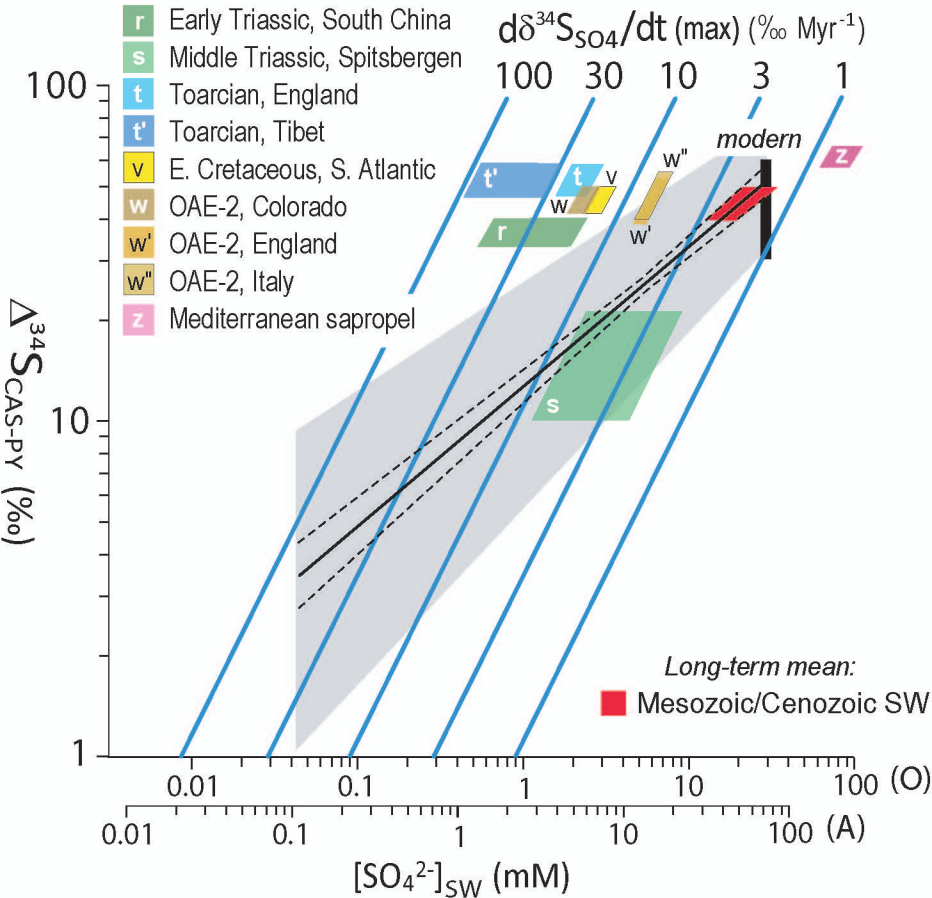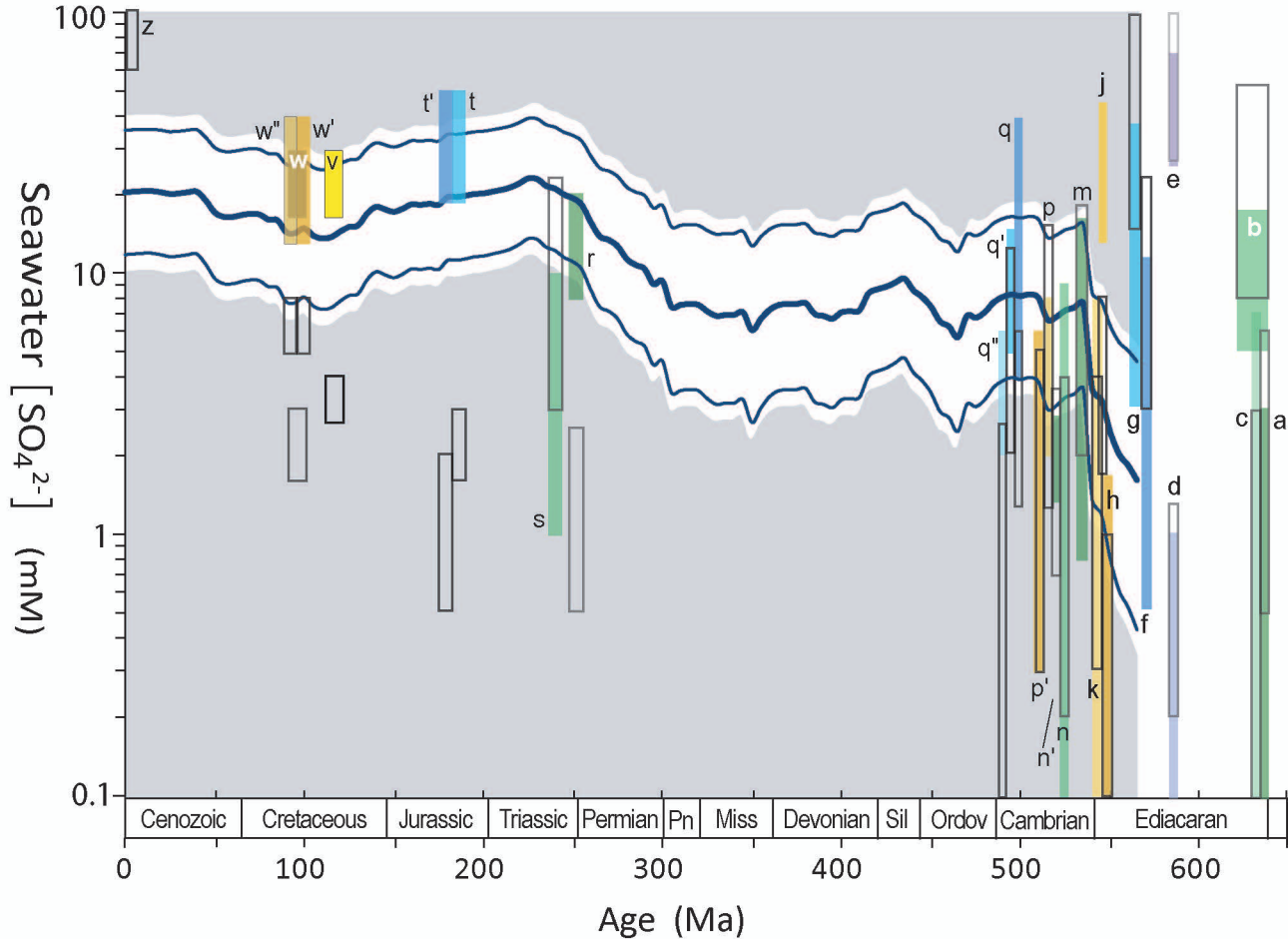
1289   Figure 4.

1290
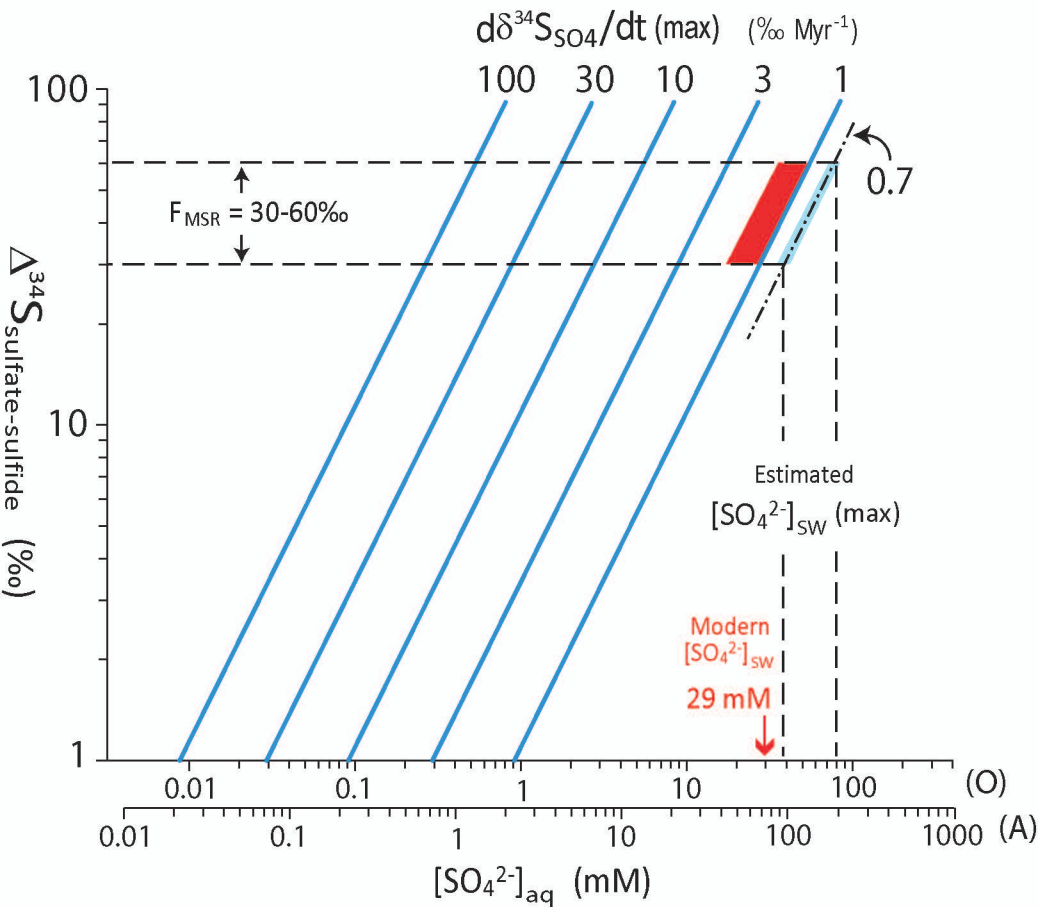
Figure 1
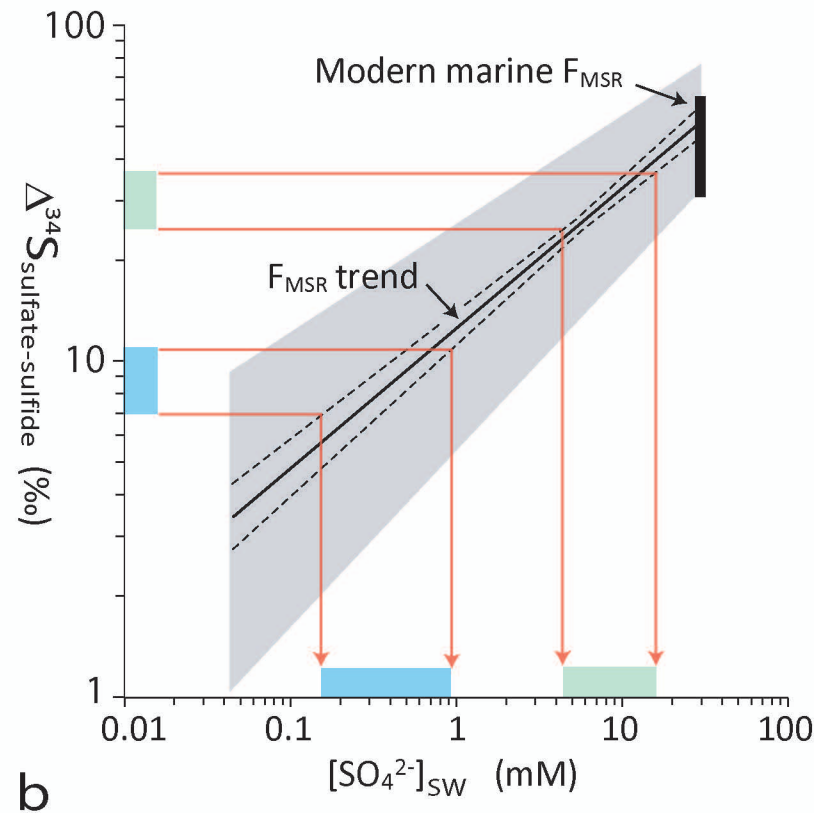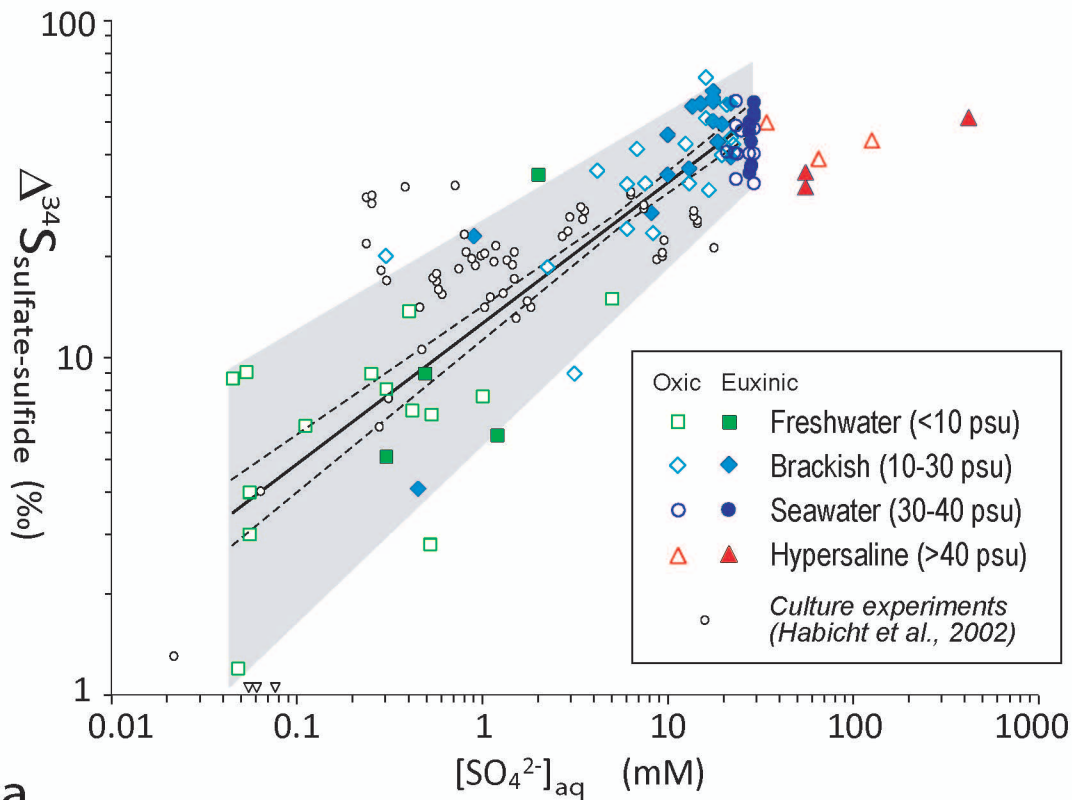
Figure 2
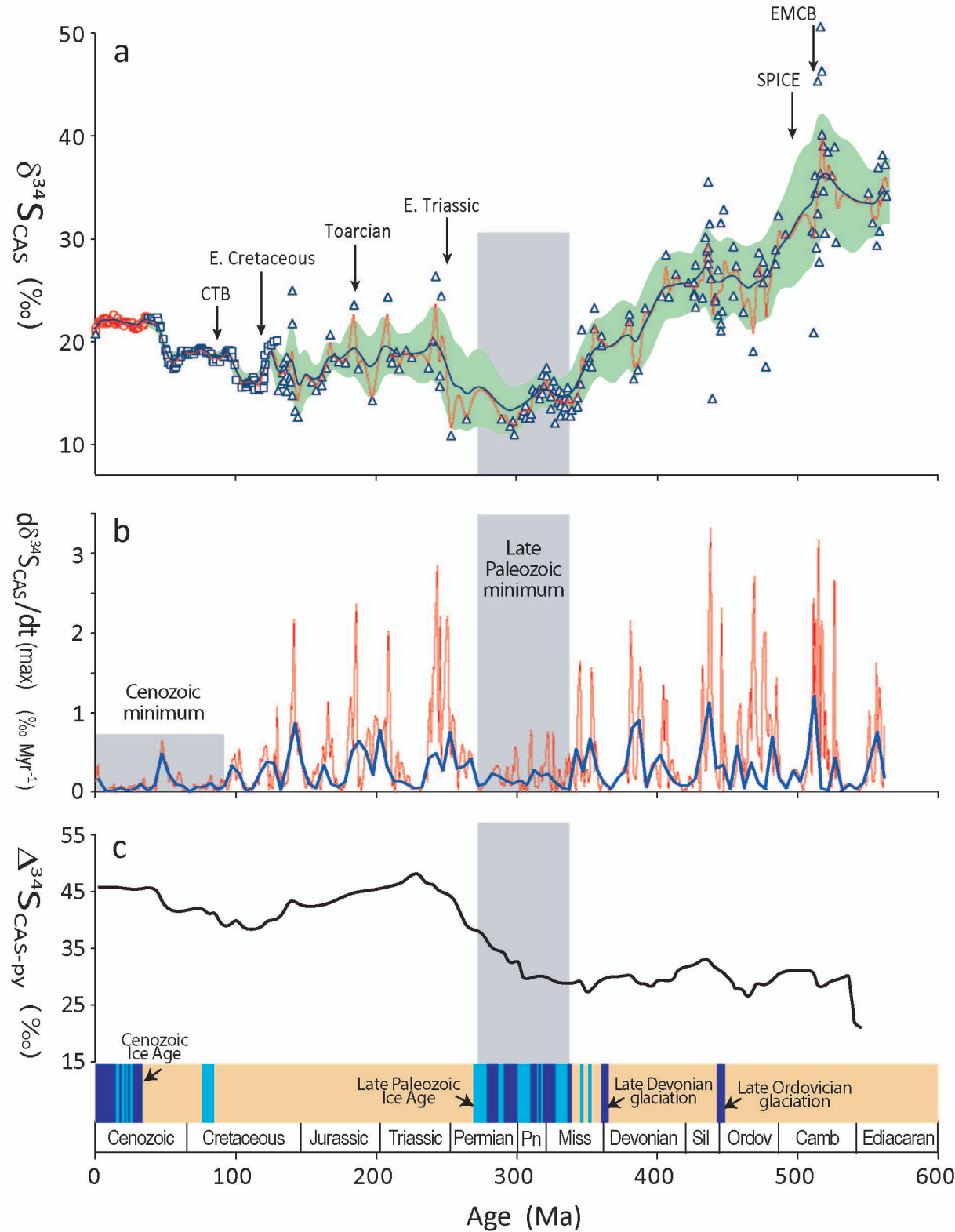
Figure 3

Figure 4

Figure 5

Legend:

- **a** Lwr Doushantuo Fm, China
- **b** Brachina Fm, Namibia
- **c** Maieberg Fm, Namibia
- **d** Sonora succession
- **e** Wonoka Fm, Australia
- **f** Sonora succession
- **g** Huqf Supergroup, Oman
- **h** Up Doushantuo Fm, China
- **j** Nama Group, Namibia
- **k** Death Valley units

Axes:
- Y-axis: $\Delta^{34}S_{CAS-PY}$ (‰)
- X-axis: $[SO_4^{2-}]_{SW}$ (mM)
- Top axis: $d\delta^{34}S_{SO4}/dt$ (max) (‰ Myr^{-1})
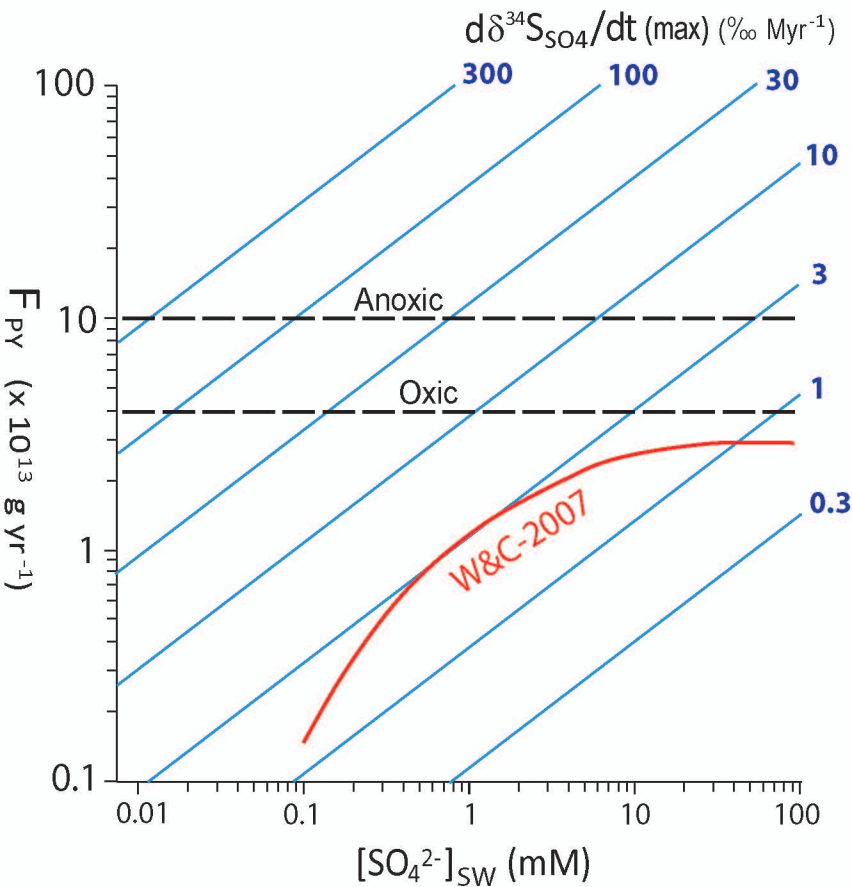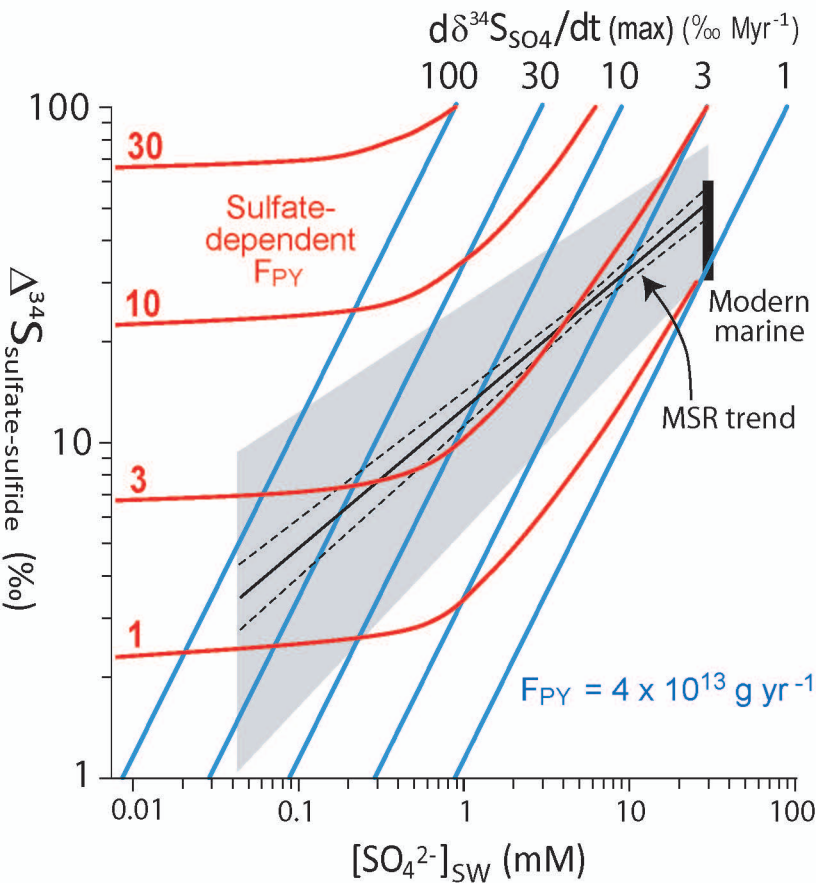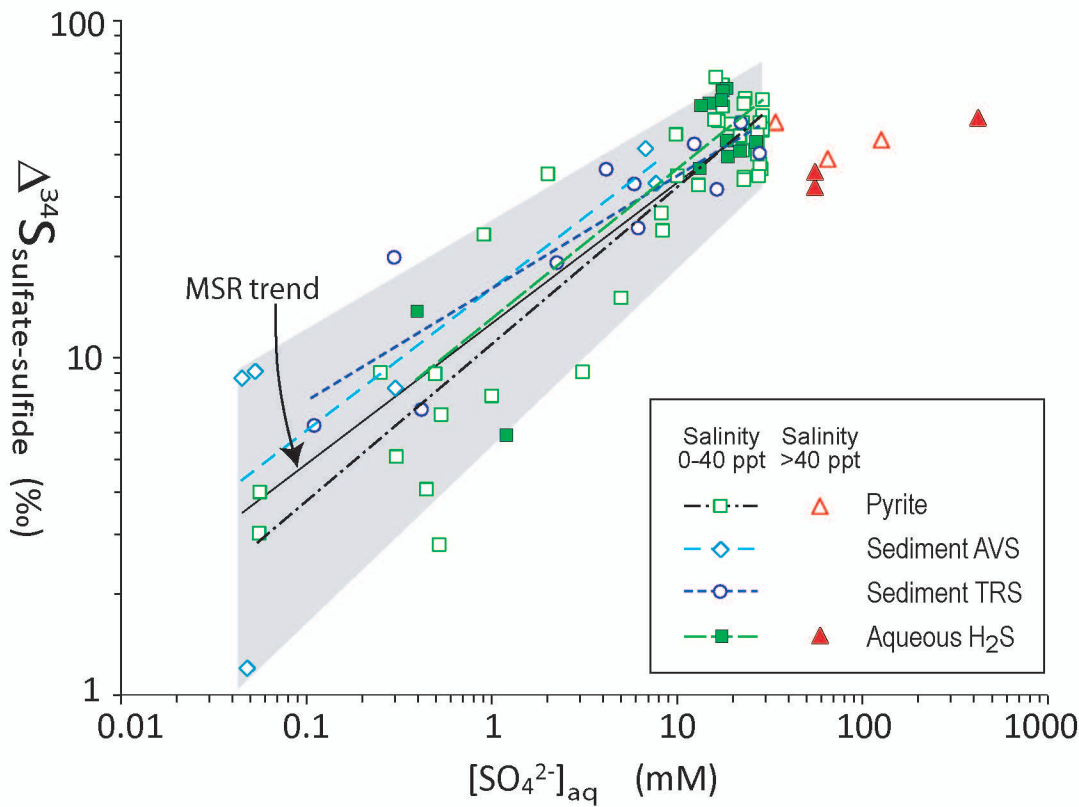
Figure 6

Figure 7

Figure 8
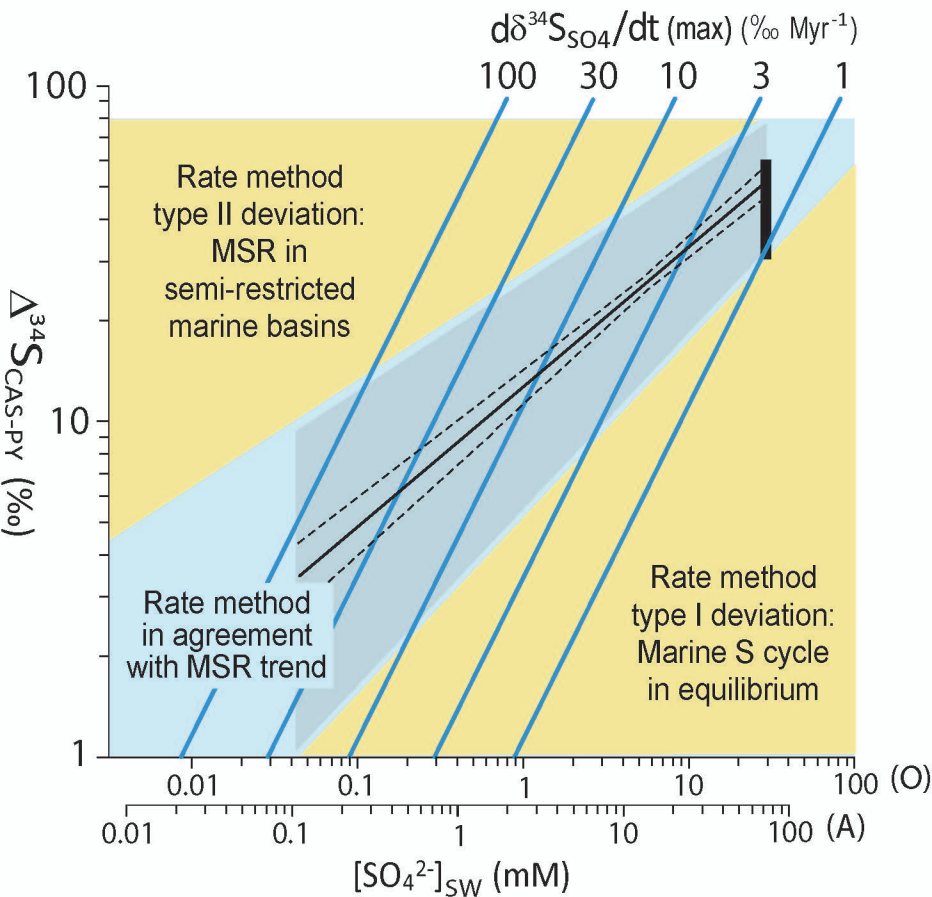
Figure 9

Figure 10

Figure B1

Figure B2

Figure B3